THE SPECTRUM OF COSMIC ELECTRONS WITH ENERGIES BETWEEN 6 AND 100 GeV

Charles A. Meegan and James A. Earl

Department of Physics and Astronomy

University of Maryland, College Park

Technical Report No. 75-019

October 1974

UNIVERSITY OF MARYLAND
DEPARTMENT OF PHYSICS AND ASTRONOMY
COLLEGE PARK, MARYLAND

Space Physics Group

THE SPECTRUM OF COSMIC ELECTRONS WITH ENERGIES BETWEEN 6 AND 100 GeV

Charles A. Meegan and James A. Earl
Department of Physics and Astronomy,
University of Maryland, College Park.

ABSTRACT

This experiment was carried out during three balloon flights which provided a total exposure of 3500 ± 60 m^2 sec sterad at an average depth of 4.8 g/cm^2. The detector, in which the development of cascade showers in a 33.7 rl absorber was sampled by 10 scintillation counters and 216 Geiger-Muller tubes, was calibrated at the Cornell Electron Synchrotron , The separation of cosmic electrons from the nuclear background was confirmed by extensive analysis of data from the flights, from the calibration and from a ground level exposure. The spectral intensity of primary cosmic ray electrons in particles/m^2 sec sterad GeV was found to have the following power law dependence upon the electron energy E in GeV:

$$dJ/dE = (800 \pm 60)E^{-3.4 \pm 0.1} .$$

Similarly, the ground level spectrum of secondary cosmic ray electrons was found to be:

$$dJ/dE = 1.1\ E^{-2.9 \pm 0.1} .$$

The steepness of the spectrum of cosmic electrons relative to that of nuclei implies one of the following conclusions: Either the injection spectrum of electrons is steeper than that of nuclei, or the electron spectrum has been steepened by Compton/synchrotron losses in the energy range covered by the experiment.

I. INTRODUCTION

Because the rate at which electrons lose energy by the Compton-synchrotron mechanism increases quadratically with energy, the energy spectrum of cosmic electrons is expected to become steeper than the injection spectrum at high energies where this mechanism becomes important. If the break energy, above which the steepening occurs, is estimated by setting the Compton-synchrotron lifetime, obtained from the density of electromagnetic energy in space, equal to the leakage lifetime of 3 Myr, obtained from cosmic ray abundances (Shapiro and Silverberg 1970), the result is $\tilde{\sim}$ 100 GeV. This expectation that the break would be found at energies well above those affected by solar modulation ($\gtrsim$ 6 GeV), has stimulated many attempts to extend to higher energies our empirical knowledge of the cosmic electron spectrum. The results of Daniel and Stephens (1966), which indicated that the electron and nuclear components have spectra of nearly identical slope up to 300 GeV, led these authors to question the existence of the universal blackbody radiation. A flat spectrum similar to that reported in this pioneering work has also been obtained by Muller and Meyer (1973). On the other hand, independent measurements (Nishimura et al. 1973; Silverberg, Ormes and Balasubrahmanyan 1973; Earl, Neely and Rygg 1972) gave a relatively steep spectrum which suggests that the Compton-synchrotron process operates upon electrons for periods longer than the conventional leakage lifetime.

The new experimental results on electrons reported here, in §V, give further documentation of a very steep spectrum. In §VI, these observations are reconciled with the data on nuclei by invoking for the volume in which cosmic rays are confined an extended region of low gas density surrounding the galactic disc. In essence, this region is a cosmic-ray halo.

The instrument, which was flown on balloons and which is described in §II, was an ionization calorimeter whose large thickness made possible a convincing identification of electron events. Specifically, the electrons appeared as a peak clearly resolved from the nuclear background. Calibrations, carried out at the Cornell Electron Synchrotron, are described in §III. Extensive tests which confirm that electrons were correctly identified are discussed in §IV.

II. APPARATUS AND BALLOON FLIGHTS

The hodoscope, shown in Figure 1, consists of 10 scintillation counters, 8 trays of Geiger - Mueller tubes, and 13 lead plates. These elements, which are 43 cm x 43 cm squares, stack up to a total thickness of 48 cm or 33.7 radiation lengths. Throughout this paper, the radiation length in lead is taken to be 5.82 g/cm^2. Each counter consists of a 0.95 cm slab of NE 102 plastic scintillator coupled by an adiabatic light pipe to a type 6655 photomultiplier. Each tray holds 27 GM tubes whose o.d. is 1.57 cm. Although all tubes are shown end-on in Figure 1, the axes of tubes in odd-numbered trays are actually perpendicular to those of tubes in even-numbered trays. This arrangement provides a crude stereoscopic description of particle trajectories. During flights, the hodoscope was kept at $\sim$ 1 atm in an aluminum capsule whose walls were 0.8 mm thick. Payload weight, including batteries, flight rack, telemetry package, etc., was $\sim$ 700 kg. The detector is similar in configuration and operation to the one employed by Earl, Neely and Rygg (1972), but its geometric factor of 352 cm^2 ster. is $\sim$ 45 times larger. For a detailed discussion of the instrument, the reader is referred to a report by Meegan (1973).

The first four trays of Geiger tubes and the first two scintillation counters make up a unit, designated hereafter as the directional filter, whose primary purpose was to specify the trajectories and the ionization rate dE/dx of incident particles. However, the directional filter also served as a guard element that helped to identify backscattered particles emerging from the lead. The other 6 counters and 4 trays, which were sandwiched among the lead plates, functioned as an ionization calorimeter that provided the information used to specify the energy of electrons and to distinguish electron showers from nuclear interactions.

When an event satisfied the triggering requirements, further triggers were inhibited during a dead time of $\sim$ 70 msec in which digital data representing the pulse height from each counter and the position of each discharged tube were transmitted at a bit rate of 8 KHz. Two overlapping triggering requirements were invoked. Events satisfying the first non-restrictive triggering criterion are designated hereafter as NRT events. They activated four-fold coincidences involving certain tubes in the directional filter which define trajectories that pass through the top and bottom of the hodoscope without going out the sides. In addition, the total number of discharges in the directional filter was required to be less than 7 for the first two flights and less than 9 for the third flight. Among the NRT events, a second restricted class, designated as RT events, satisfied a further triggering requirement of more than 5 discharges in Trays 5 and 6.

The limitation on the number of discharges in the directional filter discriminates against heavy nuclei accompanied by knock-on electrons and against interactions that send several particles through the directional filter, but in essence the first requirement was only that the geometry of the incident trajectory be suitable for analysis. Consequently, the NRT events included a large proportion of penetrating protons and helium nuclei which gave pulse height spectra characterized by peaks that provided an in-flight calibration of the scintillation counters. To obtain this information without exceeding the capacity of the telemetry system, a scaler was arranged to allow the transmission of only one in 64 NRT events. This sample was transmitted at an average rate of $\sim$ 1 event/sec.

Because the showers produced by high energy electrons tend to discharge many tubes in Trays 5 and 6, the RT class was relatively rich in events of interest here. Consequently, all RT events were transmitted at an average rate of $\sim$ 4.8 events/sec. A careful analysis of data from each flight confirmed the proper operation of two discriminators that set limits on the number of discharges in the directional filter and in the calorimeter.

Scintillation counter pulse heights were sorted into 26 channels by logarithmic pulse height analyzers. Nominally, each channel represented a factor of 1.3335, which corresponds to eight channels per decade. The r.m.s. dispersion of channel edges around their nominal values was found to be $\sim$ 0.12 channel for a typical analyzer. Thus, the accuracy of the pulse height measurements was 3.5%, the resolution was 33%, and the dynamic range covered by 26 channels was 1778.

To probe the response of the counters to minimum ionizing particles, ground level muon events were studied. The sensitivity of each counter was adjusted so that muons produced an average pulse height of about four channels. On the basis of tubes discharged, muon trajectories were then sorted according to their zenith angles and according to the points at which they penetrated the counters. When the dependence of pulse height upon these variables was analyzed for a typical counter (Counter 7), the total standard deviation of 1.87 channels around an average of 3.69 channels broke down into an r.m.s. deviation of 0.56 channel arising from the spatial dispersion of trajectories, 0.25 channel from the angular dispersion, and 1.77 channels from photoelectron statistics. This relatively insignificant effect of geometry on pulse heights was not taken into consideration

even though spatial and angular corrections could have been applied in principle. On the other hand, in the analysis of electron showers, the dependence of counter depth upon zenith angle had an important effect that is discussed in §III. In addition to the above muon runs in the NRT triggering mode, an exposure of 13,600 m^2 sec. sterad was performed outdoors at College Park, MD., under flight conditions. The ground-level spectrum of secondary electrons, reported in §V, was measured during this run.

Artificially generated light pulses of $\sim$ 5 nsec duration, were used to check on space charge limiting of the scintillation counter outputs. At the maximum pulse height, there were typical deviations from linearity of $\lesssim$ 1 channel for which corrections were applied. However, for 100 GeV electrons, only the pulse heights from the two counters nearest the shower maximum required corrections.

The experiment was flown successfully on balloons three times: twice in 1969 from Sioux Falls, South Dakota, and once in 1973 from Palestine, Texas. Flight summaries are given in table 1. During a total time at ceiling of 48.3 hrs an exposure of 3500 ± 60 m^2 sec. sterad was accumulated at an average depth of 4.8 g/cm^2. There was a second flight from Palestine on which the instrument stopped working during ascent, but throughout the flights reported here, no significant malfunctions occured.

III. CALIBRATION AND SHOWER CURVES

Because the detailed response of a lead-plastic calorimeter can not be predicted reliably on the basis of shower theory alone, a calibration was performed at the Cornell Electron Synchrotron. Data from this exposure were extrapolated with the guidance of shower theory to electron energies above 9.5 GeV, the maximum available from the accelerator. The calibration electrons were created by pair production in a thin aluminum target by a beam of bremmstrahlung photons. With the aid of a careful field mapping, the energies of these electrons could be related to their deflections by a bending magnet. The accuracy of this procedure was confirmed by the demonstration, during one run, that the maximum energy of the pair electrons was equal, within uncertainties of $\lesssim 2\%$, to the accurately known energy of the primary synchrotron beam. Information from the directional filter was invoked to specify the deflections and to ensure that the incident trajectories of accepted events were consistent with the geometry expected for electrons produced in the target. A small background due to electrons from the walls of the room was evaluated by analyzing events whose trajectories fell outside these geometrical constraints. Because the magnetic deflection gave rise to a systematic dependence of electron energy upon the spatial position of the shower axis, corrections based upon a muon mapping were applied to relate the observed pulse heights to the average expected for randomly incident electrons.

To make evident the significance of the quantities specified by calibration, it is appropriate to consider here an important parameter S which plays a crucial role in the identification of electrons and in the measurement

of their energies. This variable, defined as a sum over the eight counters in the calorimeter by the formula for the statistical χ^2 parameter

$$S\{E\} = \frac{1}{8} \sum \frac{(\text{observed pulse height} - \text{expected pulse height})^2}{(\text{standard deviation of expected pulse height})^2} ,$$

is a measure, for each event, of the agreement between the observed profile of pulse height vs. counter depth and the profile expected for electrons of energy E. The well known χ^2 function applies rigorously to S only if the pulse heights obey Gaussian statistics and are uncorrelated. In actuality, these conditions are not satisfied, but the distribution function for S nevertheless exhibits a localized peak similar to that displayed by the χ^2 distribution. The identification of electron events rests on the existence of this peak which can readily be resolved from the broad distribution of events produced by nuclei. Because it involves the pulse heights directly as recorded on a logarithmic scale, the above definition of S is convenient for the analysis of flight data. However, for the comparison of shower curves with published calculations and data and for their extrapolation upward in energy, it is more appropriate to consider an equivalent number of shower particles measured on a linear scale normalized to the pulse height for minimum ionizing mesons. This conversion is complicated, first, by the fact that the logarithm of the average number of particles is not the same as the average of the logarithm of the number of particles and, second, by the special status of the zero pulse height channel which contains all events whose pulse heights fell below a certain threshold. In expressing the results that follow in terms of equivalent numbers of shower particles, these factors were taken into account.

Figure 2 illustrates how the form of the pulse height spectrum depends upon electron energy and counter depth. Here, the thin solid and dotted lines, which refer to 3.75 GeV showers at their maximum development, give spectra before and after correction for the room background mentioned above. The background, which appears here as a peak at zero pulse height accompanied by a small tail extending up to Channel 10, has only a slight effect on the average pulse height, but it plays a more significant role in the evaluation of the standard deviation which depends quadratically upon the large difference between background and average pulse heights. Near the peak, the distribution is Gaussian, but there is a pronounced tail below the peak. This triangular form is typical of counters traversed by a large number of shower particles. In contrast, spectra for a deep counter where only a few shower particles are present, which are designated by the thick solid and dashed lines, exhibit a peak at zero pulse height corresponding to events in which charged shower particles were absent plus a second peak whose position measures the number of charged particles and whose width represents a convolution of statistical fluctuations in the number of particles with the width of the minimum ionizing peak. In the final analysis, all these details of shower behavior are summarized by the 8 average pulse heights and 8 standard deviations that enter into the calculation of S.

To obtain average pulse heights at the energies of greatest interest here, a procedure was developed that gave profiles which fit the calibration data and which behaved at higher energies qualitatively as predicted by shower theory. The description by Meegan (1973) of this procedure will not be repeated. Instead, Figure 3 summarizes the shower curves on which the

present results are based. In this context, it is worth noting that the main effect of inaccuracies in the shape of the shower curves is to broaden the electron peak in the distribution of S values. As is demonstrated below, the assignment of energy to an event depends primarily upon the area under its observed profile of ionization vs. depth. These assignments can be characterized by the ratio of electron energy to track length which was found to be 16.7 ± 0.5 MeV/rl in good agreement with Earl, Neely and Rygg (1972).

To estimate standard deviations at energies above those of the calibration, a relationship was established between the standard deviation and the average number of shower particles. This relationship is documented in Figure 4 where the standard deviations measured at the energies and depths covered by the calibration cluster with an r.m.s. dispersion of 0.3 channel about a single smooth curve (solid line). The standard deviations calculated by Nagel (1965) lie close to the same line. When the average number of particles is larger than 20, this curve approaches a constant asymptotic value of ∿1.2 channels which presumably embodies a combination of the intrinsic fluctuations with the geometric dispersion in pulse heights. When the number of shower particles is between 4 and 20 the observed points lie well above the dashed line predicted on the basis of Poisson statistics, but they are well represented by the dotted line predicted for fluctuations twice as large as Poisson. These large fluctuations, which agree with the work of Silverberg (1974), are an expected consequence of the correlations inherent in the development of showers. At the left side of Figure 4 where the average number of shower particles is much less than one, the probability of two or more particles is negligible, and the statistics can be characterized by the binomial probabilities of zero or one particles. In this regime, the relationship between the standard deviation and the

average number of particles does not depend upon the physical mechanisms that cause fluctuations. On these empirical and apriori bases, the solid curve of Figure 4 was invoked in the calculation of S as a universal relationship which did not involve energy or depth.

In the processing of each event, the electron energy E, which determines the expected pulse heights and standard deviations, was varied until the minimum value S_{min} was found. In this way, each event was assigned a nominal energy E_{nom} and a parameter S_{min} measuring the degree to which the observed profile fit an electron shower curve of energy E_{nom}. In Figure 5, the observed numbers of electron events in two Cornell runs are plotted against the parameter S_{min}. Evidently the distributions for two different energies are identical within statistical uncertainties, but they have peaks at slightly lower values of S_{min} and fall off less rapidly at high values of S_{min} than does the expected χ^2 histogram (solid line). These minor deviations from the χ^2 distribution can be attributed to the non-Gaussian form of the pulse height spectra shown in Figure 2 and to the weak anticorrelation between particle numbers reported by Brecht (1969) at separations greater than 3 rl In any case, exact knowledge of the shape of the electron peaks is not crucial because they are well resolved from the nuclear continuum (see §IV). Because of fluctuations, the nominal energies assigned to monoenergetic calibration electrons were spread over a finite interval whose r.m.s. width specifies the energy resolution of the instrument. This width decreases slowly with increasing energy from 37% at 1 GeV to 24% at 5.6 GeV.

Another important parameter that was determined during the calibration is the probability that an electron event will satisfy the RT triggering criterion by discharging more than 5 tubes in Trays 5 and 6. Figure 6 shows that this triggering probability increases rapidly with energy up to $\approx$ 5 GeV where it becomes virtually constant and equal to one. (Compare Earl, et al., 1972, Fig. 7.) Similarly, the pronounced dependence upon zenith angle θ, which appears in Figure 6 as a difference between the solid points for $\theta = 11°$ and the open points for $\theta = 26°$ and which is presumably associated with variations in the slant depth of Trays 5 and 6, becomes unimportant above 5 GeV. For analysis of flight data, the triggering probability was represented by the solid curve, which embodies a weighted average over zenith angle.

IV. IDENTIFICATION OF ELECTRON EVENTS

In Figure 7 where the number of RT events accumulated during all three flights is plotted against S_{min} for four nominal energies, the electron peaks, whose maxima occur at values of $S_{min} \approx 0.8$ comparable to those documented in Figure 5 for calibration electrons, are clearly separated from the large peaks at $S_{min} \approx 30$ which contain nuclear events whose fit to shower profiles is poor. The shape of the electron peak does not change significantly with energy, but the slope of the nuclear peak at small values of S_{min} increases with energy while its maximum moves to the right. Thus, even though the ratio of electrons to nuclei decreases from 0.045 at 10 GeV to 0.0045 at 56 GeV, the nuclear contamination at the maximum of the electron peak is quite small ($\approx$ 10%) and nearly independent of energy. The results above 6 GeV presented in §V are based upon events in the electron peaks of distributions similar to those in Figure 7. Corrections for the nuclear contamination were estimated with the aid of straight lines fitted to the distributions just above the electron peaks. The electron peaks obtained by subtracting these estimates from the flight distributions are broader than those for calibration electrons. Although slant depths corresponding to the nominal zenith angles defined by the directional filter were invoked in the calculation of S, this broadening can be attributed to dispersion within the finite angular intervals specified by the coincidence requirements and within the finite energy intervals invoked in the minimization analysis. When the important effect of dispersion in zenith angle was not taken into account, the electron peaks were relatively broad. Under these circumstances, the electron and nuclear peaks were less clearly separated than they are in Figure 7. Below 6 GeV, the electron and nuclear

peaks were not clearly resolved, because the nuclear peak is relatively broad, while electrons have only a small probability of triggering. (See Fig. 6.) Fortunately, detailed information on the shape of the electron peak was available at these energies not only from the calibration but also from a sea level exposure during which the distribution in zenith angle of triggering electrons was very similar to that during flights. To confirm the correct identification of electrons and the accurate evaluation of their energies, to validate the straight line extrapolation of the nuclear background, and to specify the shape of the electron peak, the data were examined in detail to make sure that the electron and nuclear peaks behaved as expected when certain aspects of the analysis were changed and when the conditions of exposure were varied. The paragraphs that follow describe these tests.

The key element that led to well separated electron and nuclear peaks is the thick calorimeter. To illustrate this point, Figure 8 compares the distribution of S_{min} values obtained as above from profiles measured by 8 counters (solid circles) with that obtained from profiles measured by 6 counters (open circles) in which the pulse heights in Counters 9 and 10 were not included. In the latter distribution, which is equivalent to one that would be recorded by an instrument of reduced thickness (18.7 rl vs. 33.7 rl), the electron and nuclear peaks are not resolved. However, the distributions coincide at small values of S_{min} where the electron peaks, whose shape is not sensitively dependent upon the number of counters, are dominant. Earl, et al. (1972) and Muller and Meyer (1973), who flew instruments of $\approx$ 20 rl thickness, obtained distributions similar to those represented in Figure 8 by open circles.

To display a nuclear peak uncontaminated by electrons, Figure 9 shows as solid circles an S_{min} distribution for helium nuclei identified by their ionization rate dE/dx measured in Counters 1 and 2. Although the shape of this distribution is not identical to that of the corresponding nuclear peak in Figure 7 (17.8 GeV), which presumably contains mostly protons, it exhibits at small values of S_{min} the straight line relationship that was invoked in the evaluation of background. The same dependence is confirmed by data on protons and pions (open circles) recorded during an accelerator exposure of a smaller hodoscope whose configuration was similar to the present one (Earl, et al. 1972).

The track length obtained by integrating under the observed shower profile provides a good estimate of electron energy, because virtually all of the energy carried by an incident electron is dissipated in the calorimeter. In the case of an electron event, this estimate should be consistent with the nominal energy assigned by minimizing S, for the track lengths under the shower profiles in Figure 3 are proportional to energy. But, in the case of a nuclear event, whose incident energy is not always contained and whose profile does not usually fit the shower curves, there is no reason to expect agreement between the two methods of estimating energies. These implications are explored in Figure 10 where the S_{min} distribution obtained as before for events with nominal energies near 31.6 GeV (solid circles) is compared on an absolute basis with the distribution of S values for events that were assigned energies near 31.6 GeV by multiplying their observed track lengths by the same constant, 16.7 MeV/rl, that applies to Figure 3. Evidently, the number of events in the electron peak is virtually

the same for both methods, but only about half as many nuclear events were assigned to a given energy on the basis of their track length as were assigned on the basis of their fit to shower profiles. Thus, Figure 10 shows not only that the spectral intensity of electrons is insensitive to the method of energy measurement but also that the electron and nuclear peaks respond independently to a change in procedures as is expected for two physically distinct components.

Data from the sea level exposure and from two flights at different cutoff rigidities illustrate, in Figure 11, how the shape of the electron peak was specified in the region below 6 GeV where the underlying nuclear component is more significant than it is, in Figure 7, above 6 GeV. In the distribution of S_{min} recorded at Palestine (open circles), where the cutoff at 4.5 GeV is above the nominal energy of 3.16 GeV, the peak containing reentrant albedo electrons is not resolved, because their flux is too small. At Sioux Falls (solid circles), the electron peak, which embodies a relatively large flux of primary electrons above the cutoff at 1.78 GeV, is marginally resolved. Because the energy carried by nuclear events is only partially sampled in the calorimeter, it is to be expected that the contamination at a given nominal energy comes predominantly from nuclei of higher energy. Thus, the nuclear peaks in Figure 11, in which events above cutoff are presumably dominant, are the same at different latitudes. Consequently, the dotted curve obtained by subtraction gives the shape of the electron peak, for any difference between the two flight distributions must be attributed to the electron component. At ground-level, where nuclei are rare, the main contamination arises from those few penetrating muons

that happen to satisfy the RT triggering criterion by virtue of their knock on electrons. Under these circumstances in which the background is virtually negligible, excellent agreement was obtained between the electron peak shape derived above (dotted curve) and the normalized ground-level electron peak (solid squares). On the basis of this agreement, electron intensities below 6 GeV were extracted from flight data by fitting the ground-level electron peak shapes to the left hand shoulders of the S_{min} distributions. In addition to this confirmation of electron peak shapes, the ground-level data, which are typified by the distribution shown in Figure 11, also provided a basis for the results on secondary electrons presented in §V.

In principle, tube discharges in the calorimeter trays could provide additional information on event profiles. In practice, these elements were not included in the definition of S, because the RT triggering requirements imposed on discharges in Trays 5 and 6 could bias the determination of energy, and because the extrapolation to higher energies of calibration data on tube discharges is not straightforward. Nevertheless, information on tube discharges made possible an independent check on the identification of 31.6 GeV electrons that is illustrated in Figure 12. Plotted here are S_{min} distributions for all RT events (closed circles) and for those RT events that did not discharge a tube in Tray 8 (open circles). Because 31.6 GeV showers are virtually absorbed in the 33.7 rl above Tray 8 (see Fig. 3), while one nuclear mean free path is $\approx$ 25 rl, this restriction should discriminate against nuclei and leave electrons relatively unaffected. In the distributions of Figure 12, this expected behavior appears as a depression of the nuclear peak by a factor of $\approx$ 10 due to the restriction together with no change in the electron peak. This absence of an electron

effect is somewhat surprising, because the average number of particles given at this depth by Figure 3, which is 0.5, appears to imply a 40% reduction of the electron peak. Actually, the reduction is much smaller than this prediction, because showers are dominated at large depths by low energy gamma rays which contribute significantly to the ionization recorded by a scintillation counter but which have a relatively small probability of discharging a tube.

Another test based upon tube discharges is presented in Figure 13 where the histograms giving the fraction of events vs. the number of discharges in Trays 5 and 6 at a fixed nominal energy were identical for calibration electrons (open circles) and for flight events in the electron peak (solid circles). This agreement is evidence not only for the correct identification of electrons but also for the reliability of the triggering probabilities given in Figure 6 which were computed by summing the events appearing in the calibration histograms above the triggering threshold. To extend the latter point, note that relatively few events appear just above threshold in the histogram for 17.8 GeV events in the electron peak (solid triangles). This behavior, which occurs because the peak of the histogram lies so far to the right that almost no events fall below threshold, confirms the nearly 100% triggering efficiency expected for electrons at 17.8 GeV.

V. EVALUATION OF SPECTRAL INTENSITIES

Results on the spectra of cosmic primary and ground level secondary electrons are presented at the end of this section. The basic entry in the calculation of spectra, the number of electrons falling in a specified range of energies, has been discussed above. The geometric factor will not be discussed in detail. However, it is worth noting that the geometric factor calculated on the basis of the tube diameters and tray spacings was multiplied by a correction factor of 0.91 ± 0.01 which took into account the inefficiency of the directional filter due to dead time and due to the dead spaces between tubes, and the increased efficiency associated with those events whose delta rays satisfied the coincidence requirements while the actual incident trajectory did not. After this correction was applied, the "clean flux" of all triggering particles was in excellent agreement with that measured by Rygg and Earl (1971). Because they depend upon energy, effects specific to electrons are of particular significance, for inaccuracies in the specification of these dependences lead directly to errors in the spectral index. Consequently, the synopsis that follows will describe three energy dependent corrections that were invoked and summarize their magnitudes in table 2. The report by Meegan (1973) contains a detailed exposition of how these corrections were specified by calibration data, how they were extrapolated upward in energy, and how they were confirmed by flight data.

As was discussed above, the RT triggering requirement of more than 5 discharges in Trays 5 and 6 leads to a bias against low energy electrons.

However, for electrons above 6 GeV, the selection efficiency of the RT criterion varies by only 20%, and as was documented by Figure 13, it approaches unity for electrons of sufficiently high energy. (See table 2.)

To ensure a well defined geometry for incident trajectories, it was required, in each directional filter tray, that at least one tube was discharged and that no more than two adjacent tubes were discharged. This requirement did not exclude many nuclei, for they typically cause exactly four discharges in the directional filter, one in each tray, and those particles that do penetrate the sensitive volumes of adjacent tubes or create delta rays are not excluded. In contrast, the probability that an energetic electron is excluded is relatively high for reasons which are not fully understood but which are probably related to backscattered shower particles or to the relatively high maximum energy that an ultra-relativistic electron can impart to a delta ray. The correction for this effect was determined by extrapolating to energies above 10 GeV the results of exhaustive studies of calibration events. On the basis of this procedure, which was verified by a careful analysis of flight events, the electron selection efficiency of this criterion was found to decrease from (61±5)% at 10 GeV to (30±12)% at 100 GeV. (See table 2 and Meegan, 1973, p 84.) This verification was based upon data from Flight 753 during which very few electron events were excluded by a relaxed triggering criterion that allowed up to 9 discharges in the directional filter.

To exclude heavy nuclei, the sum of the pulse heights in Counters 1 and 2 was required to be less than 14 channels. This upper limit corresponds to an ionization rate dE/dx of 2.5 times minimum. For energetic electrons, the ionization rate is expected to be 1.3 times minimum (Berger and Seltzer 1964), but the calibration data indicate and the flight data confirm that it is actually somewhat larger than expected, being $\sim$ 1.8 times minimum for 17.8 GeV electrons. Because of this enhancement, which is

presumably a further manifestation of the same effects that caused extra discharges in the directional filter, an energy dependent fraction of the incident electrons was excluded by the upper limit on dE/dx. However, this dependence on energy was weak, and the selection efficiency was greater than 70% for electrons below 100 GeV. (See table 2, and Meegan, 1973, p 86.)

Dispersion in the measurement of electron energies leads to an apparent increase in the flux at high energies, where the spectrum is steep, and to an apparent decrease at low energies, where the uncorrected spectrum has a maximum just above the instrumental cutoff. Although a correction for this effect was made, the spectral index obtained without taking it into account, 3.2 ± 0.1, was only slightly smaller than the result given below $\gamma = 3.4 \pm 0.1$. Small corrections were also applied for bremmsstrahlung and for the production of secondary electrons in the residual atmosphere above the balloon (Daniel and Stephens 1974).

Electron spectra obtained during the three flights and at ground level are summarized in Figure 14. Combined data on the primary spectrum between 6 and 100 GeV, which are given in table 3 along with the ground level data, can be described by the power law

$$\frac{dJ}{dE} = (800 \pm 60)\ E^{-3.4 \pm 0.1}$$

which corresponds to the solid line in Figure 14, and which represents a least squares fit to the data. In this equation, which characterizes our measurement of the cosmic electron spectrum, the spectral intensity dJ/dE is expressed in electrons/m^2 sec sterad GeV and the energy E is expressed in GeV. This spectrum is in excellent agreement with the results of Earl et al. (1972). The spectrum at Palestine during Flight 753 exhibits

a fairly abrupt transition from a relatively intense primary spectrum above the geomagnetic cutoff at 4.5 GeV to a less intense spectrum of re-entrant albedo below cutoff. A similar transition appears in the spectra for Flights 1277 and 1282 at the 1.8 GeV cutoff operative at Sioux Falls. At 10 GeV, the ground level spectrum lies below the primary spectrum by a factor of 230. However, this factor decreases with energy, for the spectra do not have the same slope.

In Figure 15, where the power law given above appears again as a solid line, the primary spectrum of table 3 is compared with data on high energy electrons recently published by other investigators. The situation depicted here can be described as follows: (1) From 30 to 100 GeV, the present spectral intensities are in good agreement with those quoted by Muller and Meyer (1973), but beyond 100 GeV, their data lie above the solid line on a spectrum whose index, 2.75 ± 0.1, is appreciably smaller than the one reported here. (2) Similarly, the spectrum reported by Anand, Daniel and Stephens (1973) is in fair agreement from 10 to 50 GeV, but it diverges at higher energies to follow a relatively flat spectrum whose index is 2.69 ± 0.1. (3) The spectrum reported by Silverberg, Ormes and Balasubrahmanyan (1973) is displaced above the line by a factor of 2.3 but their spectral index, 3.2 ± 0.1, is consistent with ours. (4) The results of Nishimura, et al. (1973) apply at energies above those covered here, but their spectrum, whose index is 3.2 ± 0.3, is consistent in both slope and absolute magnitude with the solid line. Thus, of five experiments, two indicate that the spectrum of cosmic electrons is comparable in slope to the spectrum of nuclei, while three indicate that it is significantly steeper. Because this contradiction is an old one that cannot be resolved here, because we trust our own results,

and because the implications of a steep electron spectrum have not been as thoroughly explored as have those of a flat spectrum, the discussion in §VI will adopt as its starting point the data in table 3.

On earth, the experimental situation is less confused than it is in the stratosphere. In Figure 16, the ground level data in table 3 (solid circles) are in good agreement not only with the experiments of Beuermann and Wibberenz (1968, open circles) but also with the calculations of Daniel and Stephens (1974, solid line). From 0.56 to 17.8 GeV, the ground level spectrum can be represented as

$$\frac{dJ}{dE} = 1.1 \quad E^{-2.9 \pm 0.1}$$

where the quantities appearing in this least squares fit to a power law have the same meaning as in the primary spectrum given above. Aside from their intrinsic significance, the ground level measurements confirm that our methods do give a relatively flat electron spectrum where one is expected. In spite of the prolonged exposures required for adequate statistical accuracy, the electron spectrum is inherently less difficult to measure on the ground than it is on balloons, because the background is less troublesome. Consequently, one can hope that, in the future, intercomparisons of this easily measured spectrum will play a role in reconciling conflicting observations of primary electrons.

VI. DISCUSSION

This section adopts the point of view that cosmic rays escape from the galaxy at a rate which is independent of residence time. Under these circumstances, the density n of electrons within the galaxy is given by the equation,

$$\frac{\partial}{\partial E} bE^2 n + \frac{n}{\tau} = PE^{-\gamma_o} , \qquad (1)$$

in which the decay of density due to energy loss, characterized by the parameter b, and due to escape, characterized by the leakage lifetime τ, is balanced by the steady injection of electrons described by a power law spectrum with coefficient P and index γ_o. Here, b measures the rate dE/dt at which an electron of energy E loses energy by the Compton-synchrotron mechanism

$$\frac{dE}{dt} = - bE^2 = - \frac{W}{307} E^2 \qquad (2)$$

where W is the electromagnetic energy density in eV/cc and where times and energies are measured in millions of years (Myr) and GeV respectively. The general solution of equation (1) embodies a gradual steepening that marks the transition from a regime in which the dominant mode of decay is leakage to one in which it is energy loss (Silverberg and Ramaty 1973). By invoking a spectrum in this transitional region, Silverberg et al. (1973) obtained a better least squares fit to their data than that given by a power law. In contrast, the power law fits our data very well ($S_{min} = 2.3$). Moreover, the steepening near 100 GeV, which is obtained when their approach is applied to our data,

contradicts available data at energies above 100 GeV. Consequently, the interpretations considered here focus upon the limiting regimes where the electron spectrum reduces to a power law.

In the first of these regimes, where the energy loss term in equation (1) is negligible compared to the leakage term, the solution is

$$n(E) = P\,\tau\,(E)\,E^{-\gamma_o} \qquad (3)$$

Although this equation presumably applies to electrons at very low energies, its chief significance here is as a description of the nuclear component. More specifically, the spectral index for high energy protons and helium nuclei (Ryan et al. 1972), $\gamma_{nuc} = 2.75 \pm 0.05$, corresponds to an index at injection $\gamma_o = 2.4$ provided that the dependence of leakage lifetime upon energy is a power law $\tau \propto E^{-0.35}$ which is a possibility suggested by recent measurements of nuclear abundances at high energies (Juliusson, Meyer and Muller 1972, Smith et al. 1973, Balasubrahmanyan and Ormes 1973). On the other hand, in the second regime where leakage is negligible, the solution is

$$n(E) = \frac{(P/b)}{(\gamma_o - 1)}\,E^{-\gamma_o - 1} \qquad (4)$$

which embodies the familiar result that the electron spectrum at high energies is one power of E more steep than the injection spectrum. If it is assumed that the index of the injection spectrum for electrons is the same as that derived above for nuclei, then the observed spectral index reported here, $\gamma_{elec} = 3.4 \pm 0.1$, has exactly the value predicted by equation (4), $\gamma_o + 1 = 2.4 + 1 = 3.4$. Thus we interpret the observed spectrum of electrons as a fully steepened one reflecting an equilibrium between injection and energy loss.

However, the electron spectrum is steepened only above a break energy E_{br},

$$E_{br} = \frac{153}{(\gamma_o - 0.35)W\,\tau} \quad , \qquad (5)$$

which evidently must be less than 6 GeV. If W = 1 eV/cc, this implies that $\tau > 12$ Myr which is not compatible with the widely quoted value $\tau = 3$ Myr (Shapiro and Silberberg 1970) obtained by assuming a constant density of of 1 H atom/cc over the mean path length of 3 g/cm^2 traversed by cosmic rays near 3 GeV. To resolve this contradiction, we suggest that the confinement volume V for cosmic rays extends above and below the galactic disc to include a region of reduced gas density where the Compton-synchrotron mechanism is operative but where the probability of nuclear interactions is small. Consequently, the leakage lifetime derived from nuclear abundances is increased by a factor $\gtrsim V/V_{disc.}$ which can be estimated by invoking the lower limit on τ derived above

$$\frac{V}{V_{disc}} > \frac{12\ \text{Myr}}{3\ \text{Myr}} = 4.$$

Thus, for a 0.5 Kpc layer of gas (Jackson and Kellman 1974), this minimum requirement is satisfied by a disc shaped confinement volume of 2 Kpc thickness, but greater thicknesses, ranging up to a full fledged galactic halo, are not ruled out. This indication that cosmic rays propagate freely throughout a relatively large volume surrounding the galaxy provides a motivation for attempting to refine the model developed by Jokipii and Meyer (1968) which incorporates this feature. On the other hand, it is possible that the observed electron spectrum results from an equilibrium, described by equation (3), between leakage and the injection of a spectrum of electrons whose index, $\gtrsim 3.1$, is substantially larger than that for nuclei. In this case, the elusive steepening of the electron spectrum is still to be found at energies well above 100 GeV.

This research, which was supported by the National Aeronautics and Space Administration under grant NGR 21-002-066, is based upon work submitted to the University of Maryland in partial fulfillment of the requirements for the Doctor of Philosophy degree in Physics. Computer time was provided by NASA through the Computer Science Center at the University of Maryland. Balloon flights were carried out under the auspices of ONR and NCAR. The staff at the Cornell Electron Synchrotron provided invaluable assistance during the calibration. George Umberger built the instrument. Hundreds of excellent Geiger-Muller tubes were constructed by Larry Votta, Ron Lindsay, Amy Werba and Gail Robbins. The extensive contributions of Larry Bagg and Tom Rygg to all phases of this investigation are gratefully acknowledged. Our thanks also go to Dr. S. Alfred Stephens for many useful suggestions and interesting conversations.

TABLE 1

BALLOON FLIGHTS

Flight Number	1277	1282	753
Date	9 Sept. 1969	24 Sept. 1969	17 May 1973
Launch Time (UT)	0046	0251	0007
Ceiling (UT)	0440	0740	0308
End of Data (UT)	1950	2159	2200
Geomagnetic Cutoff (GeV/c)	1.8	1.8	4.5
Altitude (mbar)	4.7	5.2	4.4
Geometric Factor (m^2 ster)	.0335 ± .0007	.0328 ± .0007	.0362 ± .0007
Corrected Exposure (m^2 sec ster)	1085 ± 30	958 ± 30	1488 ± 40
Total Number of RT events	85,742	175,499	283,281

TABLE 2

ENERGY DEPENDENT ELECTRON SELECTION EFFICIENCIES

Electron Energy (GeV)	Criterion		
	RT Triggering	Directional Filter Discharges	(dE/dx) $\leq$ 14 channels
.56	.02 ± .01	.85 ± .05	.974 ± .004
1.00	.08 ± .03	.82 ± .04	.967 ± .004
1.78	.25 ± .06	.79 ± .04	.957 ± .006
3.16	.55 ± .05	.75 ± .04	.944 ± .010
5.62	.82 ± .02	.68 ± .04	.926 ± .014
10.0	.95 ± .03	.61 ± .05	.90 ± .02
17.8	1	.54 ± .06	.87 ± .03
31.6	1	.46 ± .07	.84 ± .04
56.2	1	.38 ± .09	.79 ± .05
100	1	.30 ± .12	.72 ± .08

TABLE 3

SPECTRAL INTENSITIES IN (electrons/m^2 sec sterad GeV)

Combined Flights		Ground Level	
Energy*	Intensity	Energy*	Intensity
6.42	(1.3 ± 0.3)	.56	(4.8 ± 1.0)
11.4	$(2.2 \pm 0.3) \times 10^{-1}$	1.00	(1.3 ± 0.3)
20.3	$(3.2 \pm 0.5) \times 10^{-2}$	1.78	$(2.7 \pm 0.3) \times 10^{-1}$
36.1	$(5 \pm 1) \times 10^{-3}$	3.16	$(6.6 \pm 0.7) \times 10^{-2}$
64.1	$(6 \pm 2) \times 10^{-4}$	5.62	$(8.9 \pm 0.8) \times 10^{-3}$
114	$(3 \pm 2) \times 10^{-5}$	10.0	$(1.4 \pm 0.2) \times 10^{-3}$
		17.8	$(2.2 \pm 0.6) \times 10^{-4}$

*Intensities quoted are based on the number of electrons with energies falling in a logarithmic interval spanning the range from 0.75 E_o to 1.33 E_o, where E_o is the energy in this column. However, corrections for the effects of averaging over this finite interval were applied in such a way that differential intensities presented in this table refer to the energy E_o.

REFERENCES

Anand, K.C., R.R. Daniel, and S.A. Stephens 1973, Conference Papers, 13th Int. Conf. Cosmic Rays, Denver, 1, 355.

Balasubrahmanyan, V.K., and J.F. Ormes 1973, Ap. J., 186, 109.

Berger, M.J. and S.M. Seltzer 1964, Tables of Energy Losses and Ranges of Electrons and Positrons, NASA SP-3012.

Beuermann, K., and G. Wibberenz 1968, Can. J. Phys., 46, S1034.

Brecht, J.J. 1969, M.S. Thesis, University of Maryland.

Daniel, R.R., and S.A. Stephens 1966, Phys. Rev. Letters, 17, 935.

Daniel, R.R., and S.A. Stephens 1974, Rev. Geophys. and Space Sci., 12, 233.

Earl, J.A., D. Neely, and T. Rygg 1972, J. Geophys. Res., 77, 1087.

Jackson, P.D., and S.A. Kellman 1974, Ap. J., 190, 53.

Jokipii, J.R., and P. Meyer 1968, Phys. Rev. Letters, 20, 752.

Juliusson, E., P. Meyer and D. Muller 1972, Phys. Rev. Letters, 29, 445.

Meegan, C.A. 1973, Ph.D. thesis, University of Maryland, available as Tech. Report No. 74-055.

Muller, D., and P. Meyer 1973, Ap. J., 186, 841.

Nagel, H. 1965, Z. fur Physik, 186, 319.

Nishimura, J., M. Matsuo, T. Ishii, T. Kobayashi, K. Yokoi, K. Niu, and T. Taira 1973, Conference Papers, 13th Int. Conf. Cosmic Rays, Denver, 5, 3073.

Ryan, M.J., J.F. Ormes, and V.K. Balasubrahmanyan 1972, Phys. Rev. Letters, 28, 985.

Rygg, T.A., and J.A. Earl 1971, J. Geophys. Res., 76, 7445.

Shapiro, M., and R. Silberberg 1970, Ann. Rev. Nucl. Sci., 20, 323.

Silverberg, R.F. 1974, Ph.D. Thesis, University of Maryland.

Silverberg, R.F., J. Ormes, and V.K. Balasubrahmanyan 1973, J. Geophys. Res., 78, 7165.

Silverberg, R.F., and R. Ramaty 1973, Nature Phys. Sci., 243, 134.

Smith, L.H., A. Buffington, G.F. Smoot, L.W. Alvarez, and M.A. Wahlig 1973 Ap. J., 180, 987.

JAMES A. EARL

Department of Physics and Astronomy
University of Maryland
College Park, Maryland 20742

CHARLES A. MEEGAN

Department of Space Physics and Astronomy
Rice University
Houston, Texas 77001

FIGURE CAPTIONS

Figure 1. Schematic diagram of the hodoscope. Geiger-Muller tubes in the four trays of the directional filter are numbered.

Figure 2. Pulse height spectra for electron events recorded during the calibration. The curves defined by square data points refer to 3.75 GeV showers sampled by Counter 5 at 4.6 rl near their maximum development where the average number of equivalent shower particles $\langle N \rangle = 22$. The thin solid and dotted curves give, respectively, spectra before and after correction for room background. Showers sampled by Counter 7 at a depth of 14 rl, well past their maximum, give spectra designated by open circles and a dashed line for 3.75 GeV electrons, and by solid circles and a thick solid line for 1.0 GeV electrons. In the latter spectra, which correspond to relatively small average numbers of equivalent shower particles, many events give zero pulse height which indicates the absence of ionizing radiation.

Figure 3. Shower curves invoked in this paper for the analysis of electron events. The ordinate corresponds to the ratio of observed pulse height to the pulse height produced by ground level muons. Data points give results from the accelerator exposure.

Figure 4. Standard deviations calculated on the basis of pulse height distributions similar to those in Figure 2 and plotted against the average number of equivalent shower particles cluster around a universal curve (solid line). At the left where the probability of two or more particles is small, this curve does not depend upon the mechanisms that cause fluctuations. At the right, where many shower particles are present, the standard deviations follow the dotted curve which corresponds to fluctuations twice those of the Poisson distribution.

Figure 5. For calibration electrons, the distribution of number of events vs. the parameter S_{min} displays a well defined peak. However, because of correlations among pulse heights, and because of the non-Gaussian form of the pulse height distributions, this peak does not coincide with the statistical χ^2 distribution.

Figure 6. Below 10 GeV, the probability that an electron will satisfy the restrictive triggering criterion is a rapidly varying function of energy and zenith angle. However, this probability approaches unity for electrons with energy above 6 GeV.

Figure 7. In the distributions giving the number of RT events recorded during flights vs. S_{min}, the electron peaks at $S_{min} \lesssim 0.8$ are clearly resolved from the nuclear peaks at $S_{min} \lesssim 30$.

Figure 8. If the two deepest counters are not included in the calculation of S_{min}, the electron and nuclear peaks are not clearly resolved.

Figure 9. Neither the S_{min} distribution for helium nuclei recorded during flights nor that for protons and pions recorded during a calibration display any trace of an electron peak near $S_{min} = 0.8$.

Figure 10. A change in the method of determining electron energies affects the nuclear peak but not the electron peak.

Figure 11. At 3.16 GeV, geomagnetism has a pronounced effect on the electron peak and no effect on the nuclear peak. At ground level, the electron peak is clearly resolved because the background due to muons is relatively small.

Figure 12. The requirement that there be no discharges in Tray 8 has a pronounced effect on the nuclear peak and no effect on the electron peak.

Figure 13. Histograms which give the number of events vs. the number of discharges in Trays 5 and 6. At 6 GeV, identical histograms were obtained above the RT triggering threshold for calibration electrons and for flight electrons. At 17.8 GeV, the histogram is displaced toward larger multiplicity.

Figure 14. Above 6 GeV, the spectral intensities from three flights are all consistent with a single power law, but at lower energies, cutoff effects are evident. The ground level spectrum (dashed line) is less intense than the primary spectrum by a factor of $\approx$ 200.

Figure 15. A compilation of independent measurements of the primary electron spectrum at high energies.

Figure 16. The ground level spectrum of secondary cosmic ray electrons.

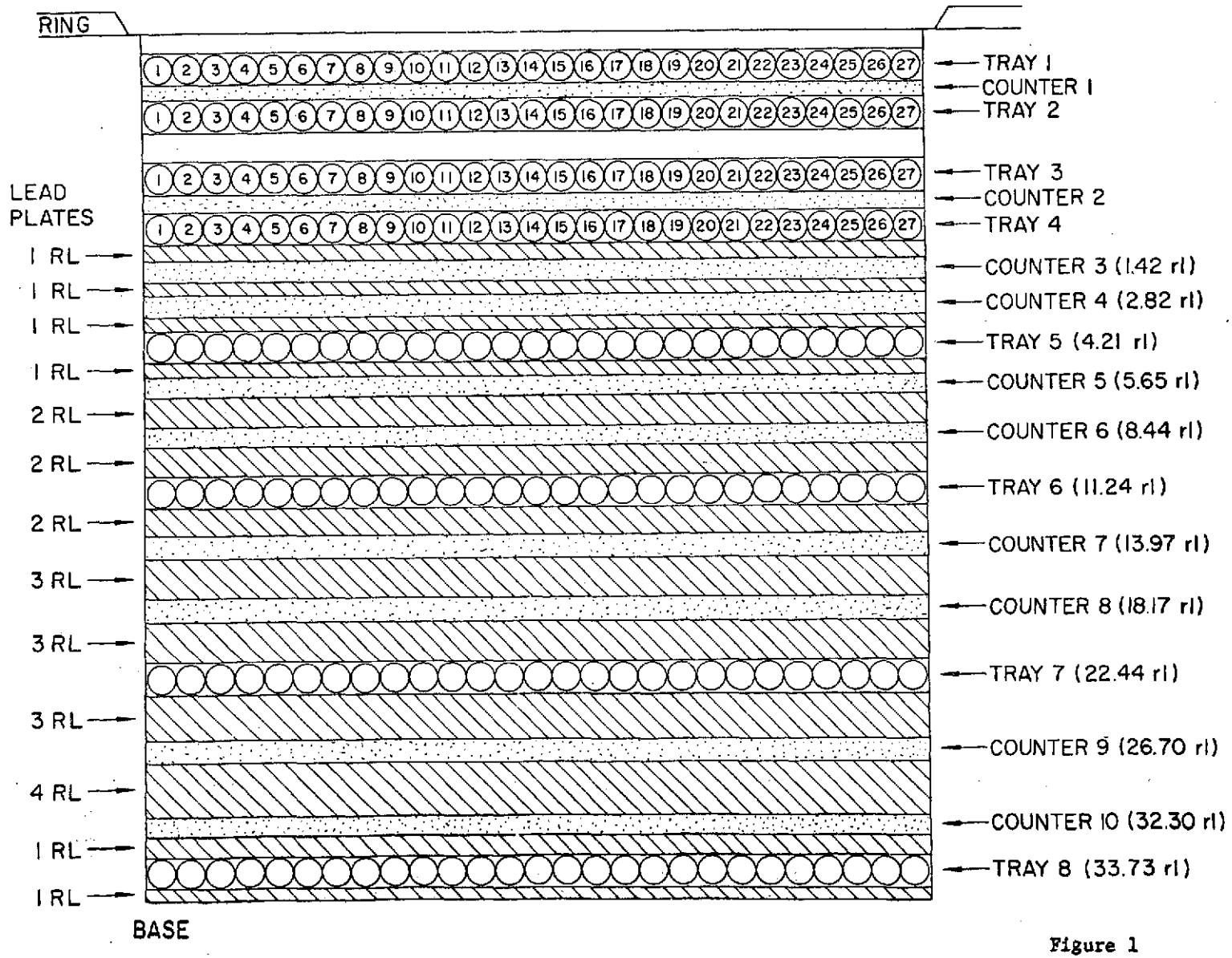
RING
LEAD PLATES
1 RL
1 RL
1 RL
1 RL
2 RL
2 RL
2 RL
3 RL
3 RL
3 RL
4 RL
1 RL
1 RL
BASE
TRAY 1
COUNTER 1
TRAY 2
TRAY 3
COUNTER 2
TRAY 4
COUNTER 3 (1.42 rl)
COUNTER 4 (2.82 rl)
TRAY 5 (4.21 rl)
COUNTER 5 (5.65 rl)
COUNTER 6 (8.44 rl)
TRAY 6 (11.24 rl)
COUNTER 7 (13.97 rl)
COUNTER 8 (18.17 rl)
TRAY 7 (22.44 rl)
COUNTER 9 (26.70 rl)
COUNTER 10 (32.30 rl)
TRAY 8 (33.73 rl)

Figure 1

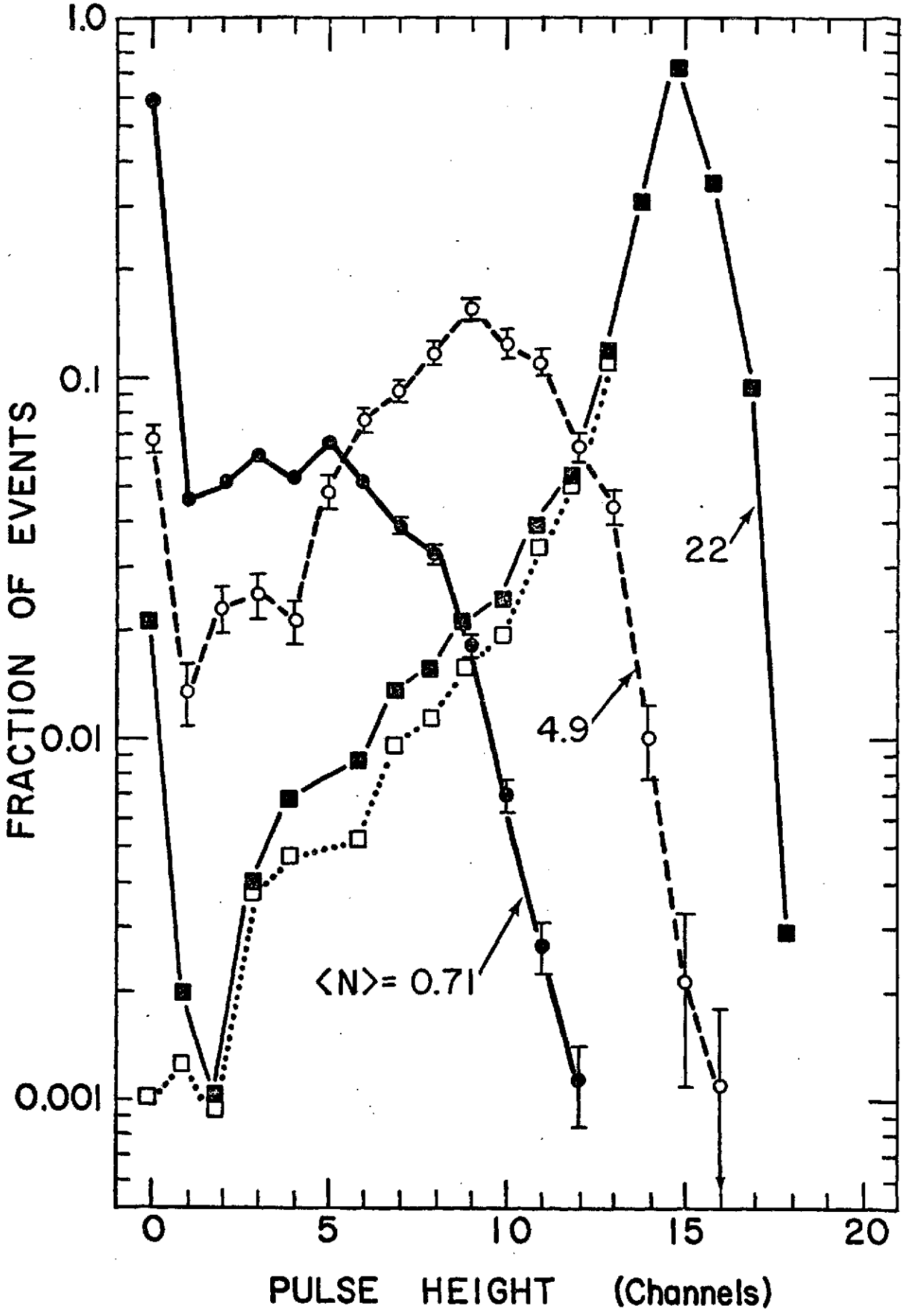
1.0
0.1
0.01
0.001
FRACTION OF EVENTS
22
4.9
<N>= 0.71
0
5
10
15
20
PULSE HEIGHT (Channels)

Figure 2

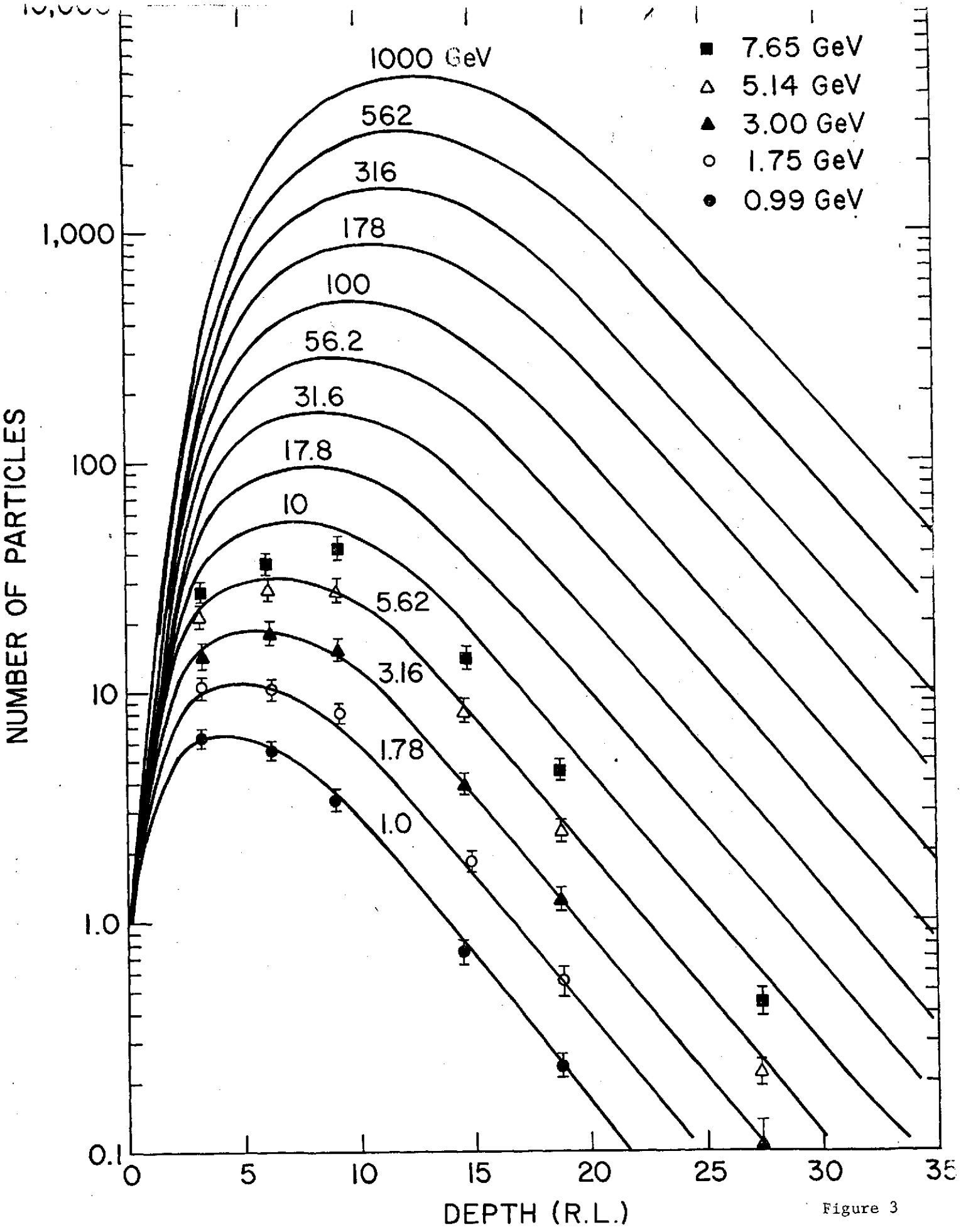
1000 GeV
562
316
178
100
56.2
31.6
17.8
10
5.62
3.16
1.78
1.0
7.65 GeV
5.14 GeV
3.00 GeV
1.75 GeV
0.99 GeV
NUMBER OF PARTICLES
1,000
100
10
1.0
0.1
0
5
10
15
20
25
30
35
DEPTH (R.L.)

Figure 3

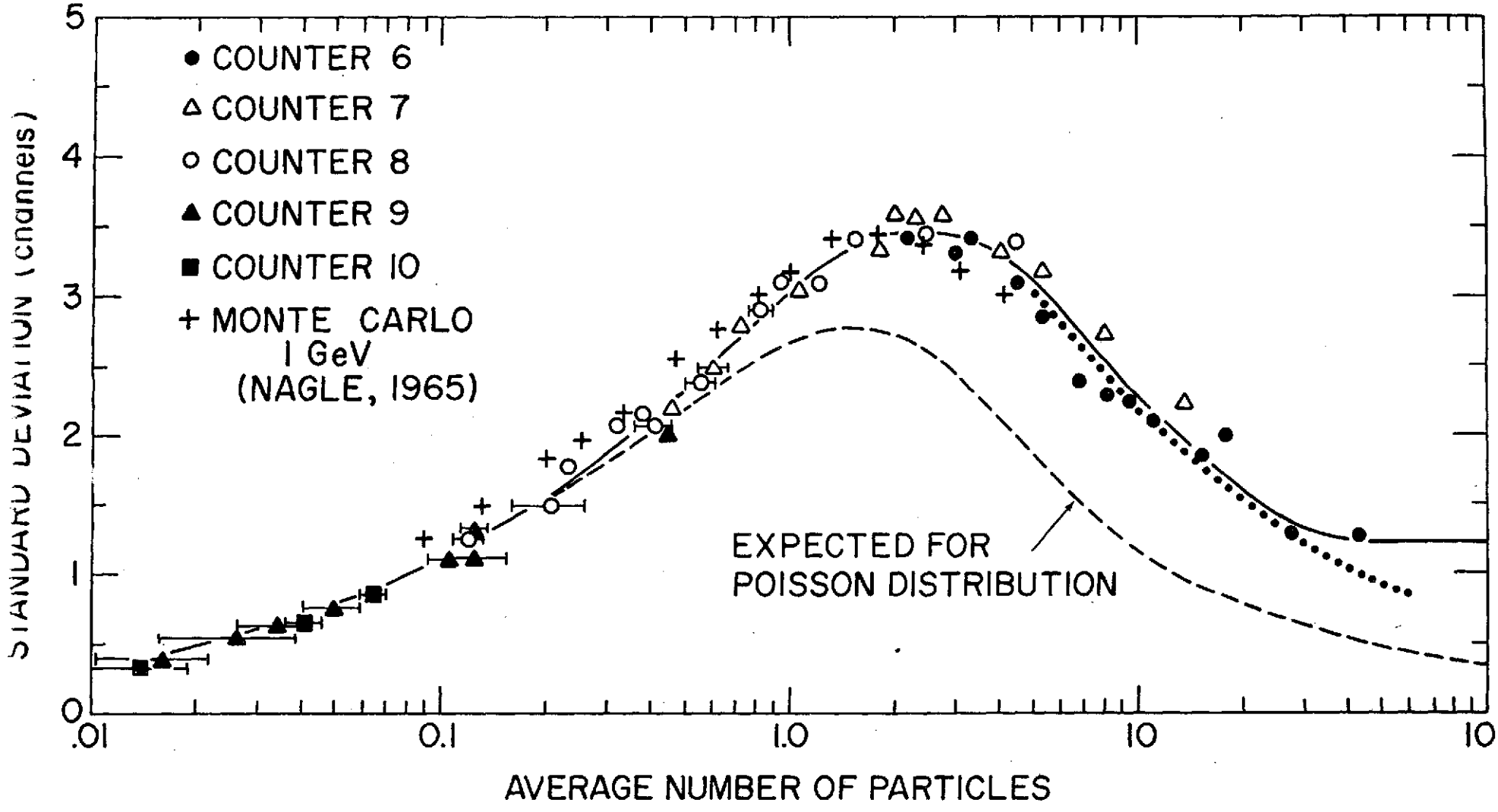
COUNTER 6
COUNTER 7
COUNTER 8
COUNTER 9
COUNTER 10
MONTE CARLO
1 GeV
(NAGLE, 1965)
EXPECTED FOR
POISSON DISTRIBUTION
STANDARD DEVIATION (channels)
AVERAGE NUMBER OF PARTICLES
0
1
2
3
4
5
.01
0.1
1.0
10
10

Figure 4

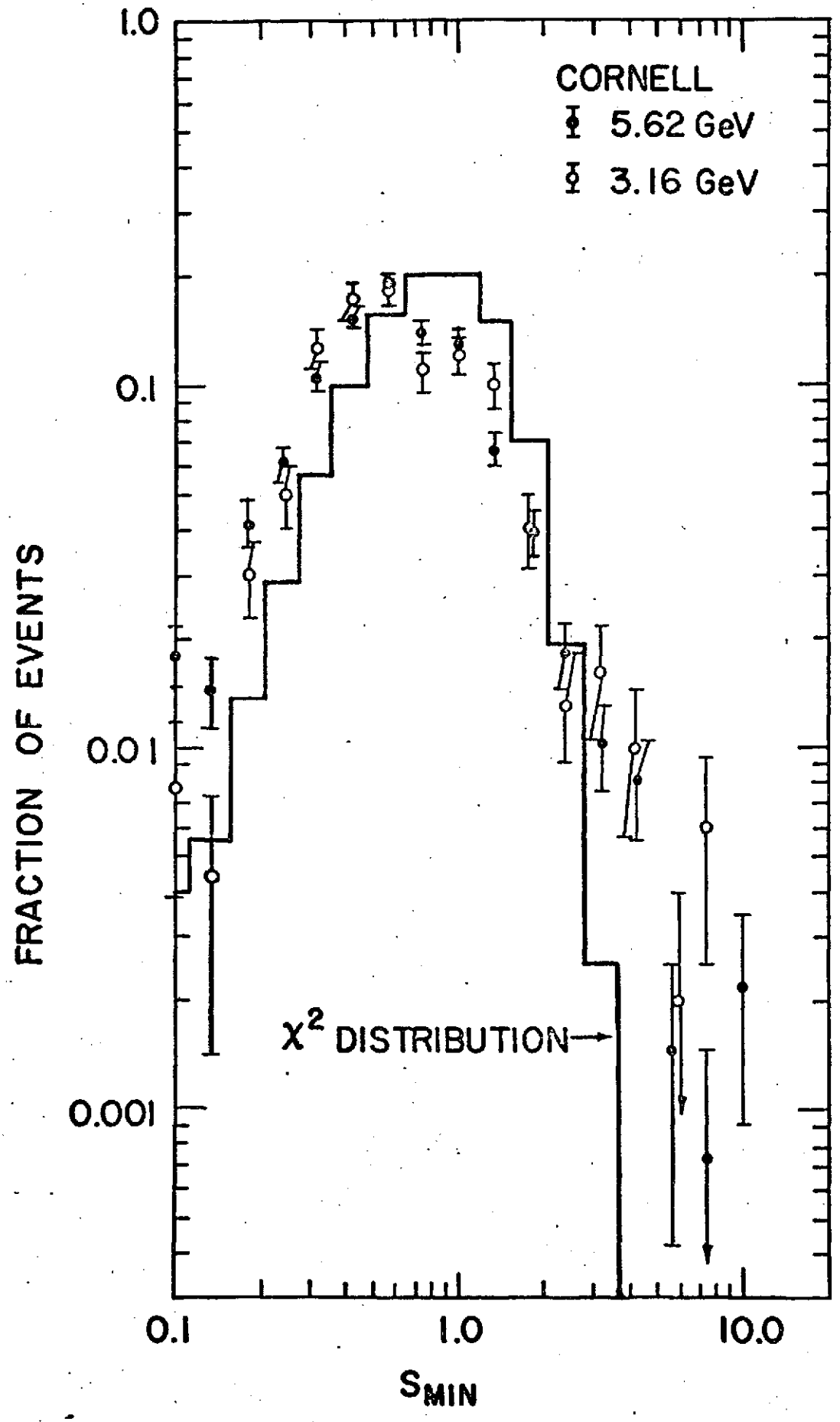
CORNELL
5.62 GeV
3.16 GeV
1.0
0.1
0.01
0.001
FRACTION OF EVENTS
χ² DISTRIBUTION
0.1
1.0
10.0
SMIN

Figure 5

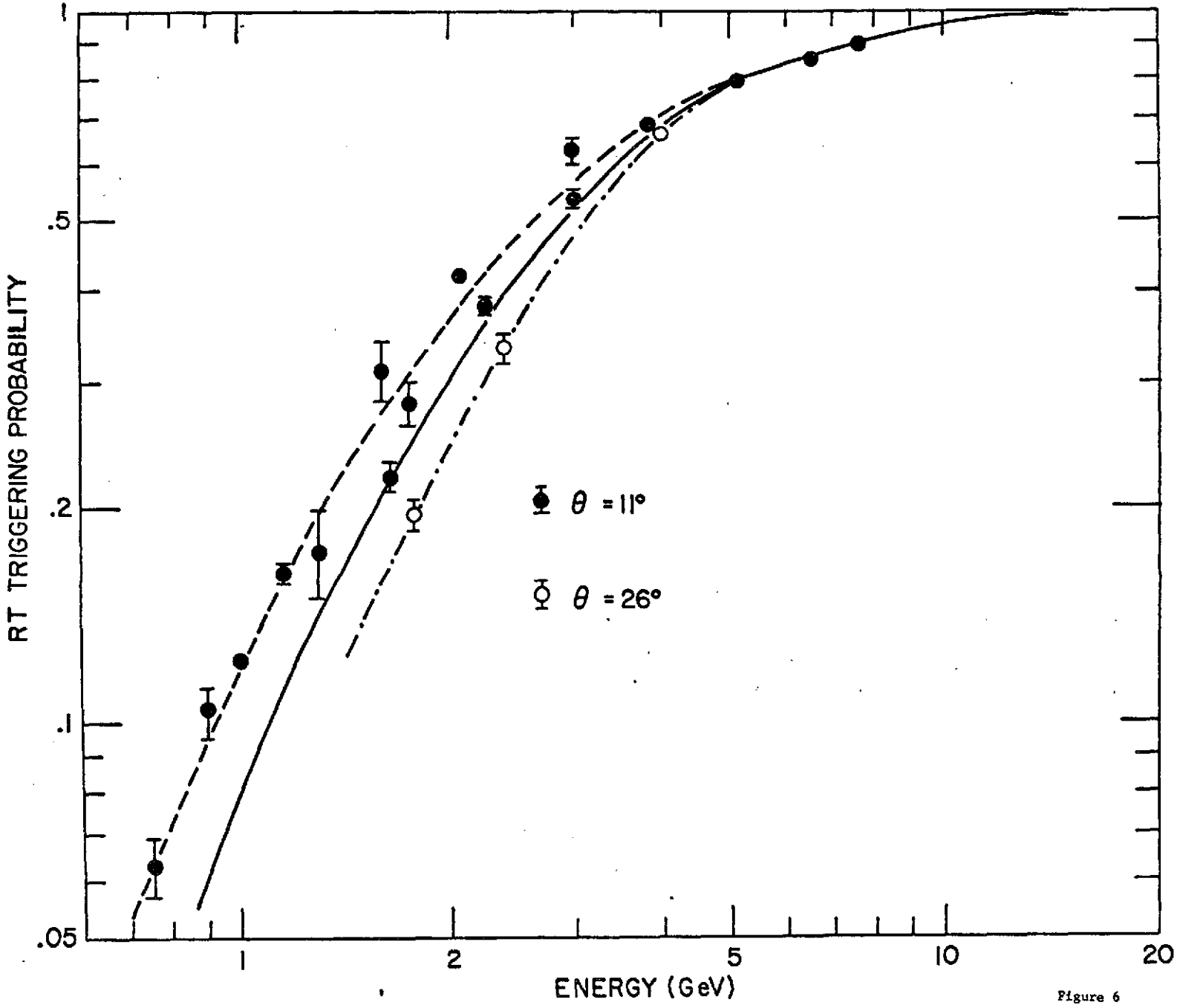
RT TRIGGERING PROBABILITY
1
.5
.2
.1
.05
1
2
5
10
20
ENERGY (GeV)
θ = 11°
θ = 26°

Figure 6

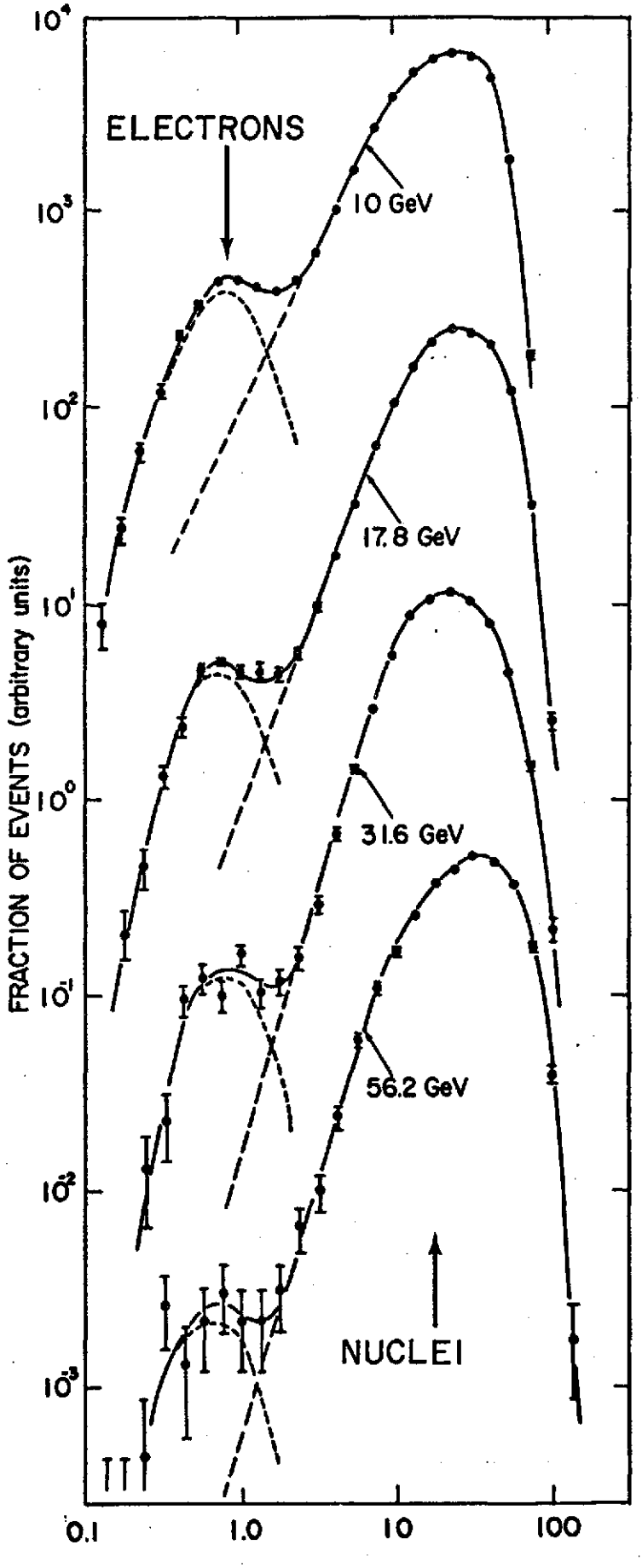
ELECTRONS
10 GeV
17.8 GeV
31.6 GeV
56.2 GeV
NUCLEI
FRACTION OF EVENTS (arbitrary units)
S_{MIN}
0.1
1.0
10
100

Figure 7

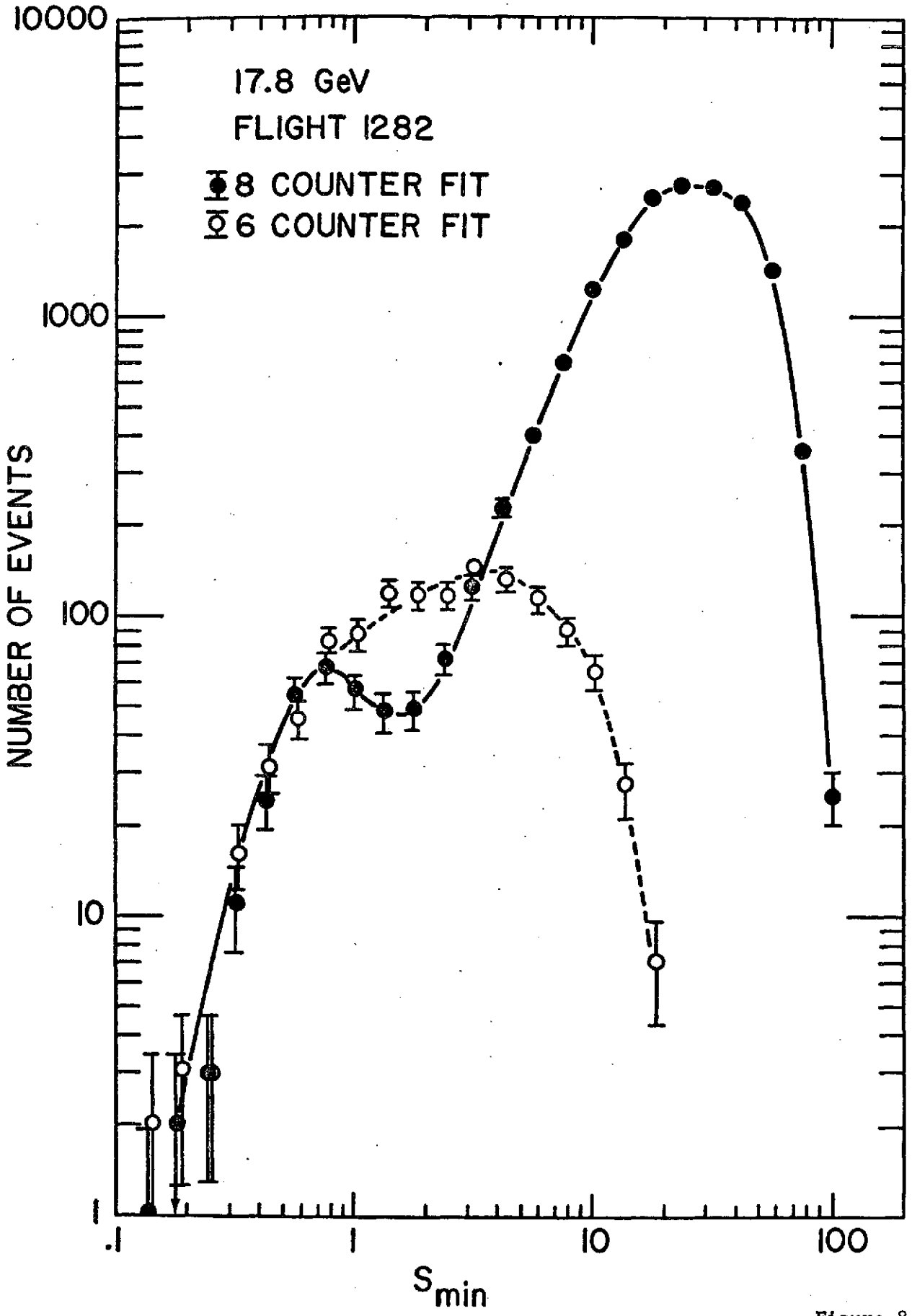
10000
1000
100
10
1
NUMBER OF EVENTS
17.8 GeV
FLIGHT 1282
8 COUNTER FIT
6 COUNTER FIT
.1
1
10
100
S_{min}

Figure 8

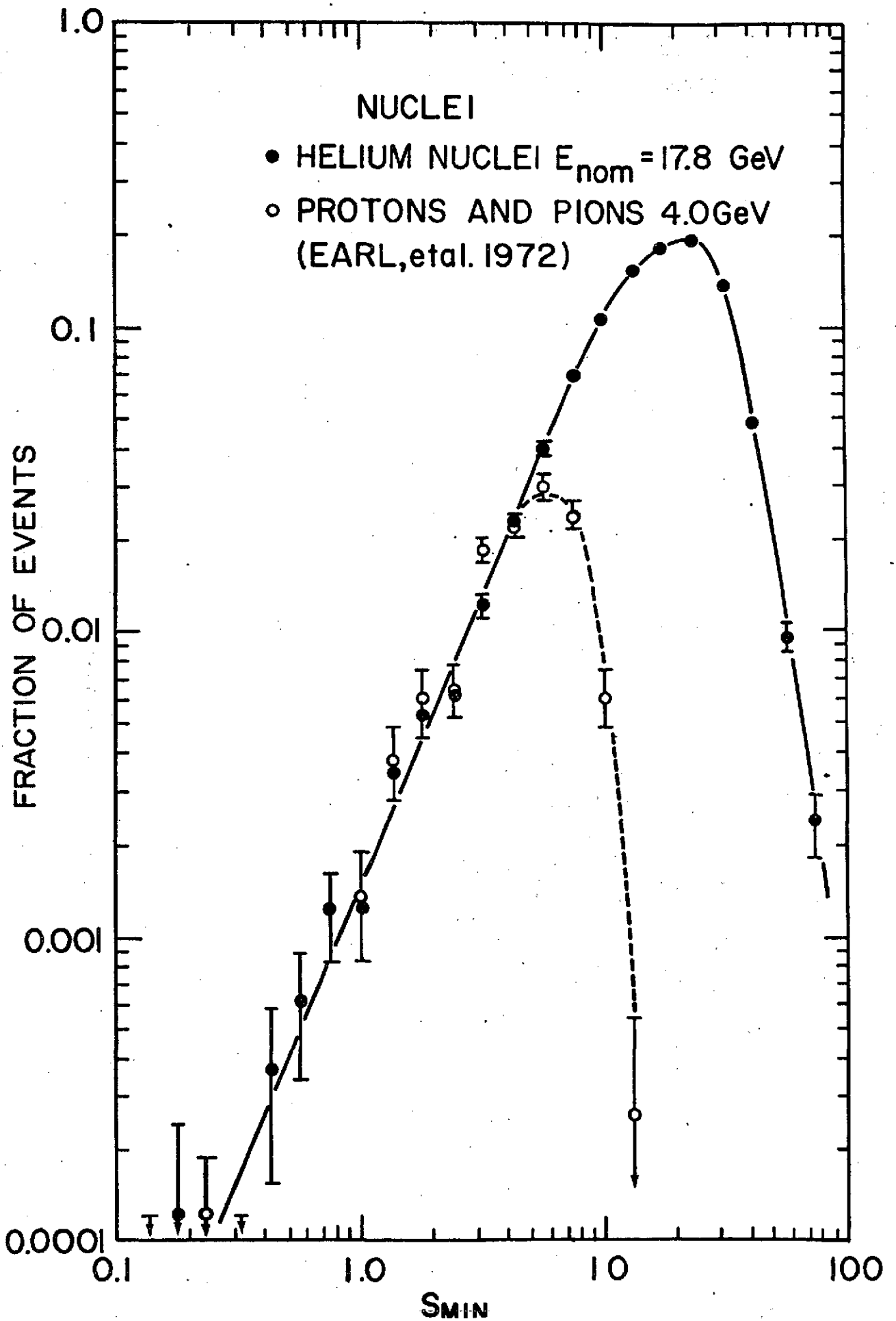
NUCLEI
HELIUM NUCLEI E_{nom} = 17.8 GeV
PROTONS AND PIONS 4.0GeV
(EARL, etal. 1972)
FRACTION OF EVENTS
1.0
0.1
0.01
0.001
0.0001
0.1
1.0
10
100
SMIN

Figure 9

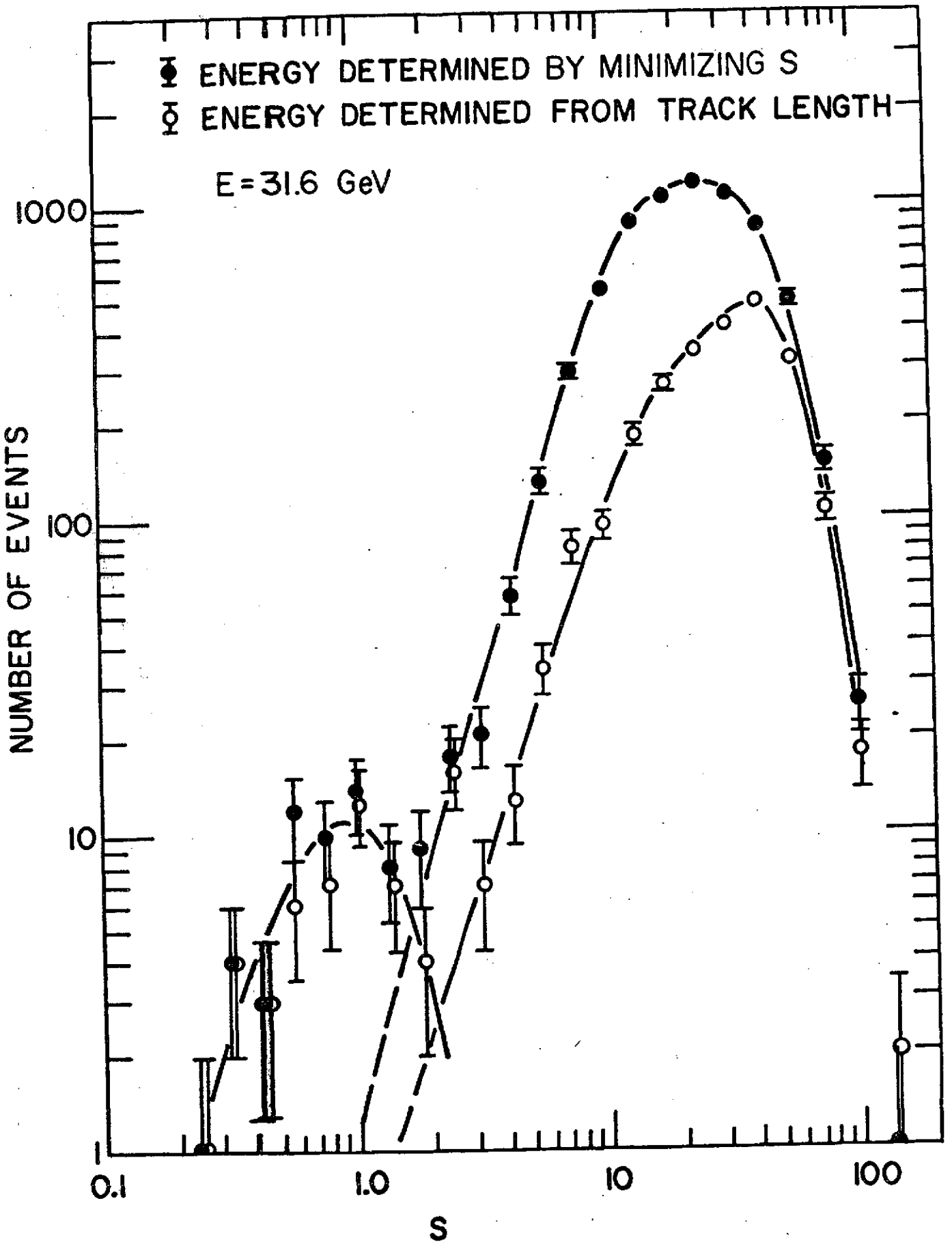
ENERGY DETERMINED BY MINIMIZING S
ENERGY DETERMINED FROM TRACK LENGTH
E=31.6 GeV
NUMBER OF EVENTS
1000
100
10
1
0.1
1.0
10
100
S

Figure 10

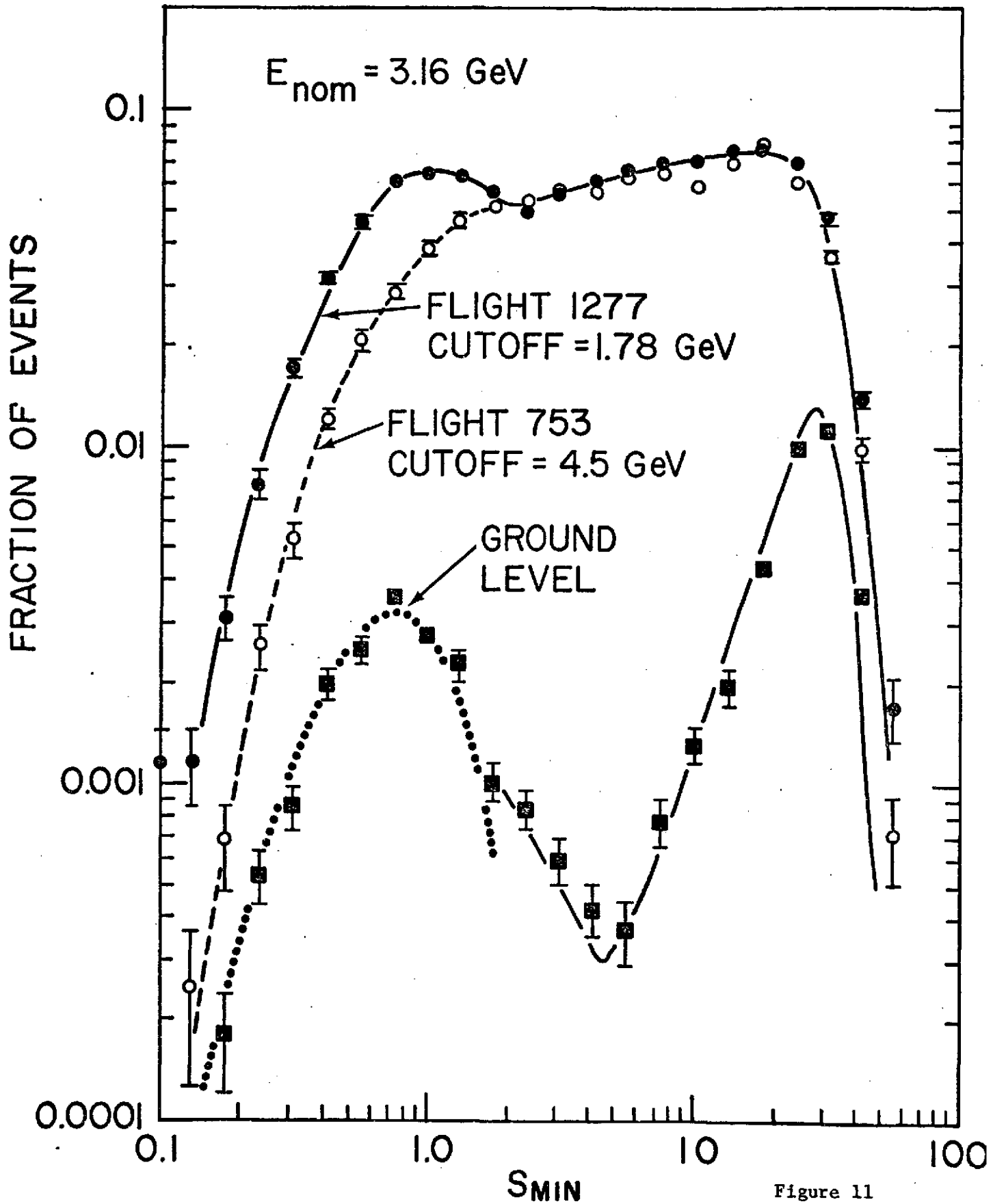
E_{nom} = 3.16 GeV
FLIGHT 1277
CUTOFF = 1.78 GeV
FLIGHT 753
CUTOFF = 4.5 GeV
GROUND
LEVEL
FRACTION OF EVENTS
0.1
0.01
0.001
0.0001
0.1
1.0
10
100
S_{MIN}

Figure 11

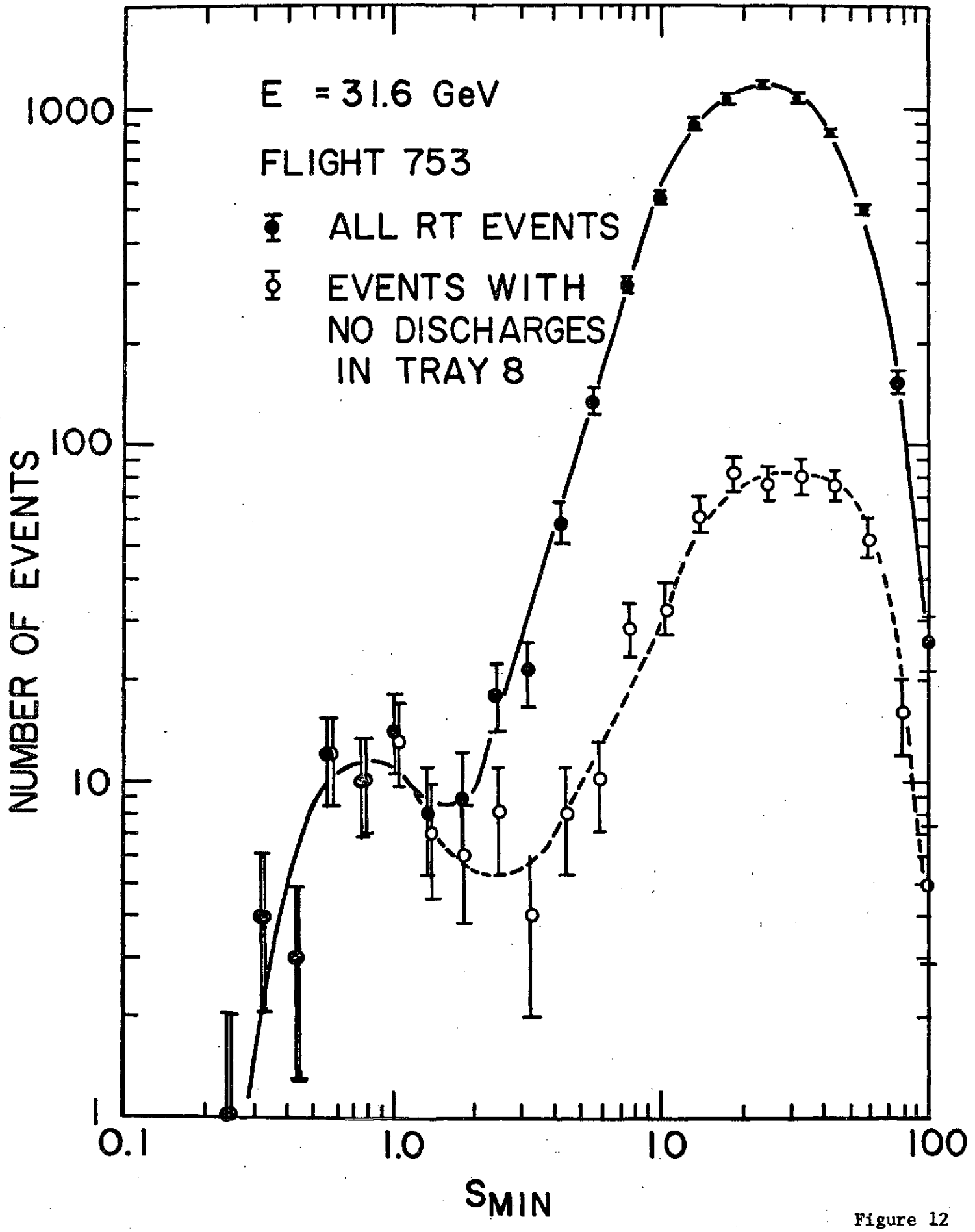
E = 31.6 GeV
FLIGHT 753
ALL RT EVENTS
EVENTS WITH NO DISCHARGES IN TRAY 8
NUMBER OF EVENTS
1000
100
10
1
0.1
1.0
10
100
SMIN

Figure 12

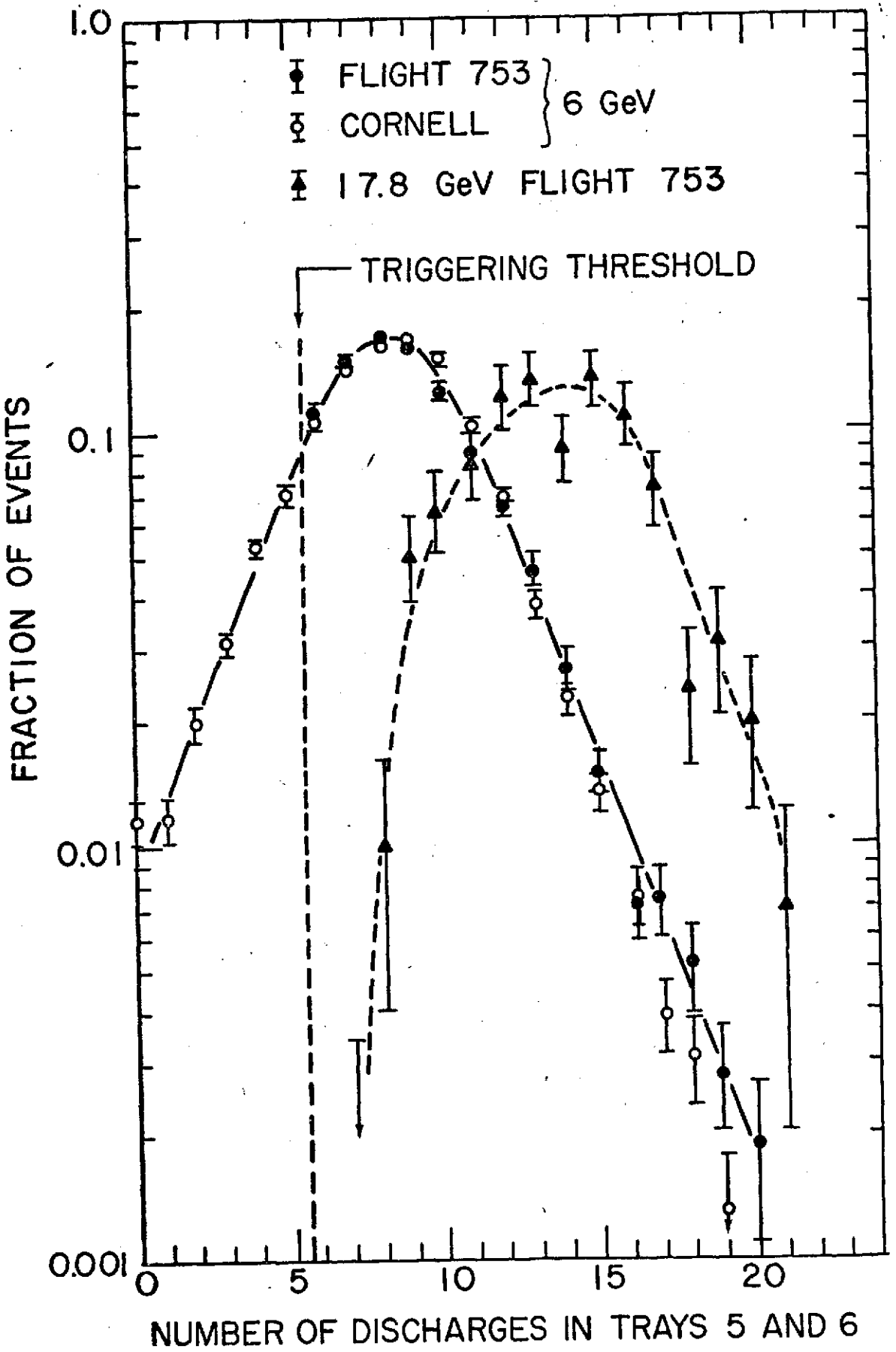
1.0
0.1
0.01
0.001
FRACTION OF EVENTS
FLIGHT 753
CORNELL
6 GeV
17.8 GeV FLIGHT 753
TRIGGERING THRESHOLD
0
5
10
15
20
NUMBER OF DISCHARGES IN TRAYS 5 AND 6

Figure 13

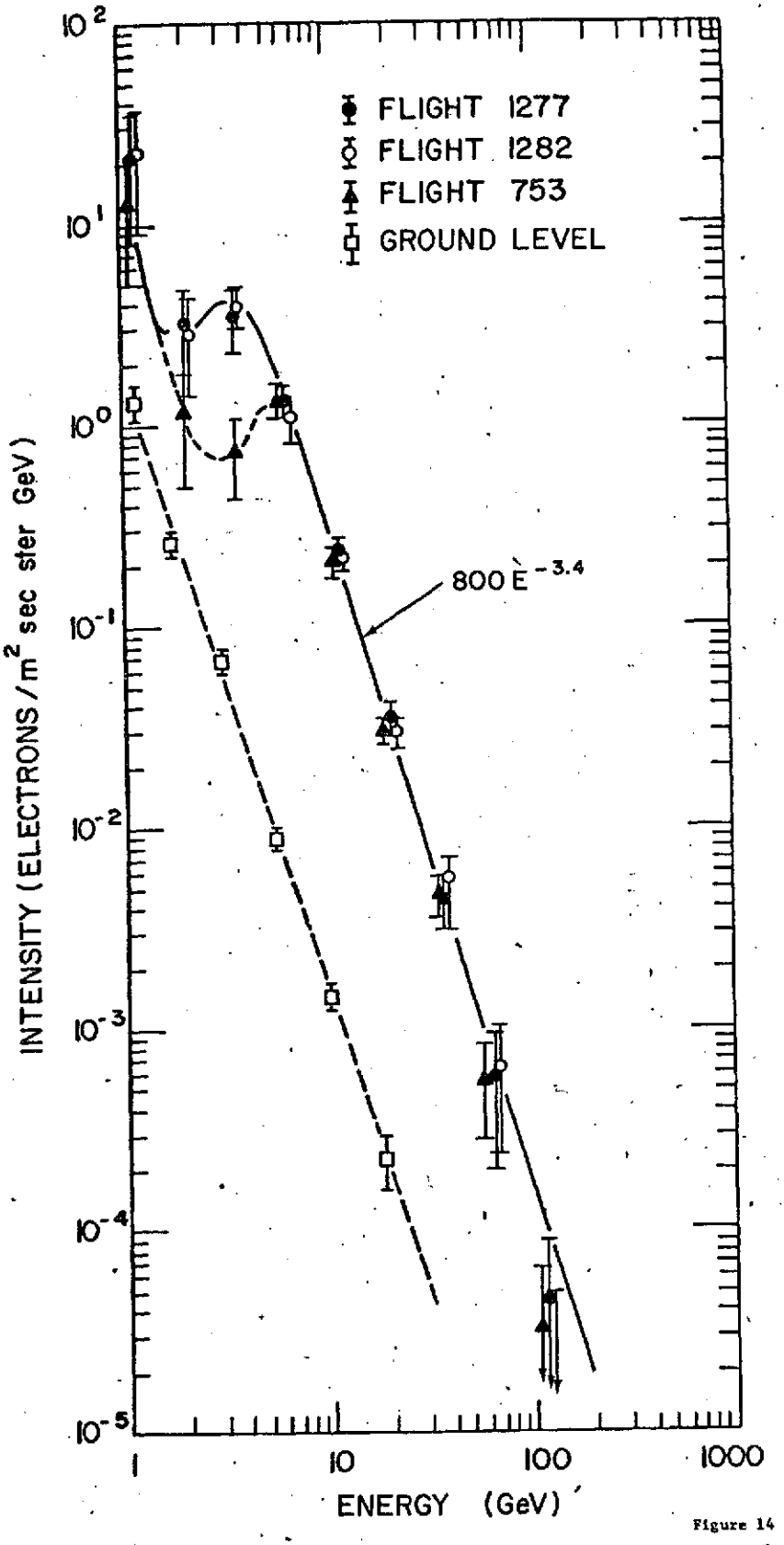

Figure 14

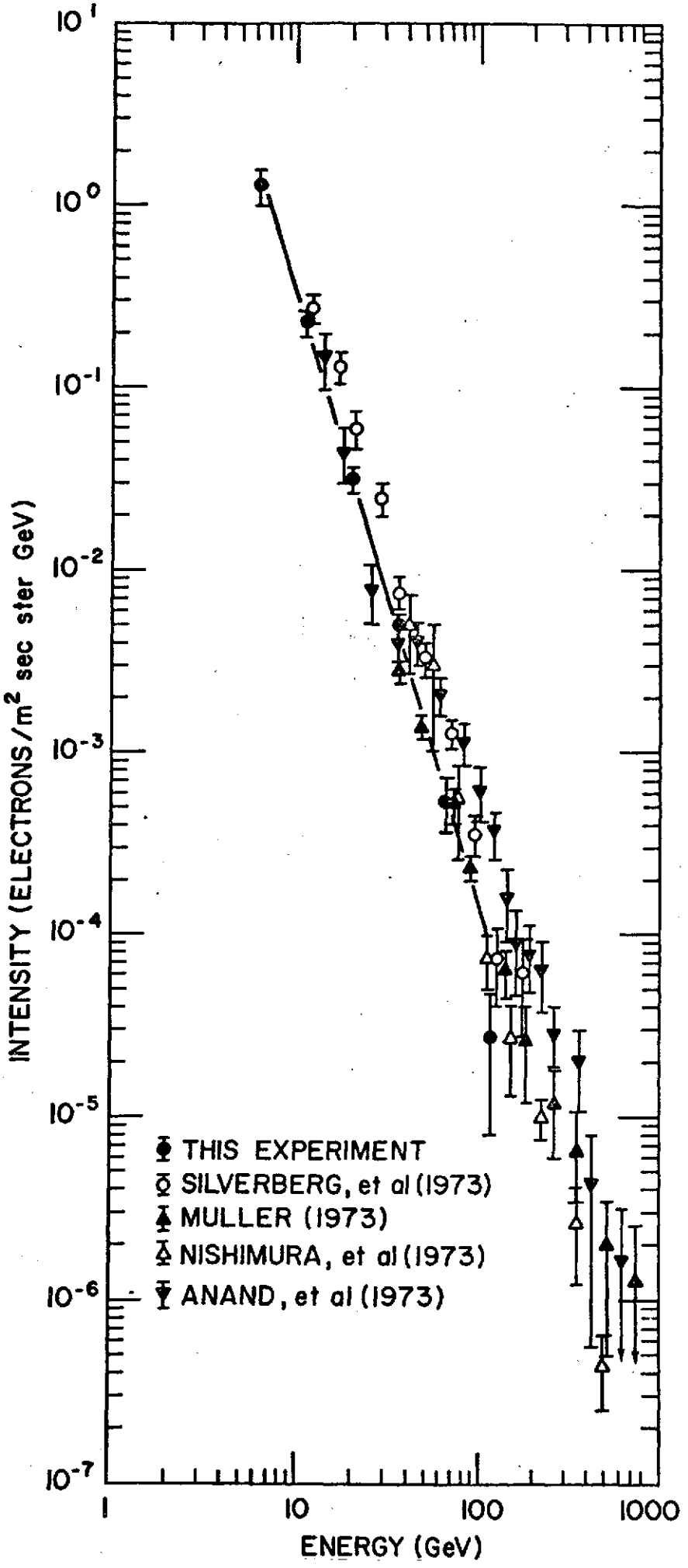
INTENSITY (ELECTRONS/m² sec ster GeV)
ENERGY (GeV)
THIS EXPERIMENT
SILVERBERG, et al (1973)
MULLER (1973)
NISHIMURA, et al (1973)
ANAND, et al (1973)

Figure 15

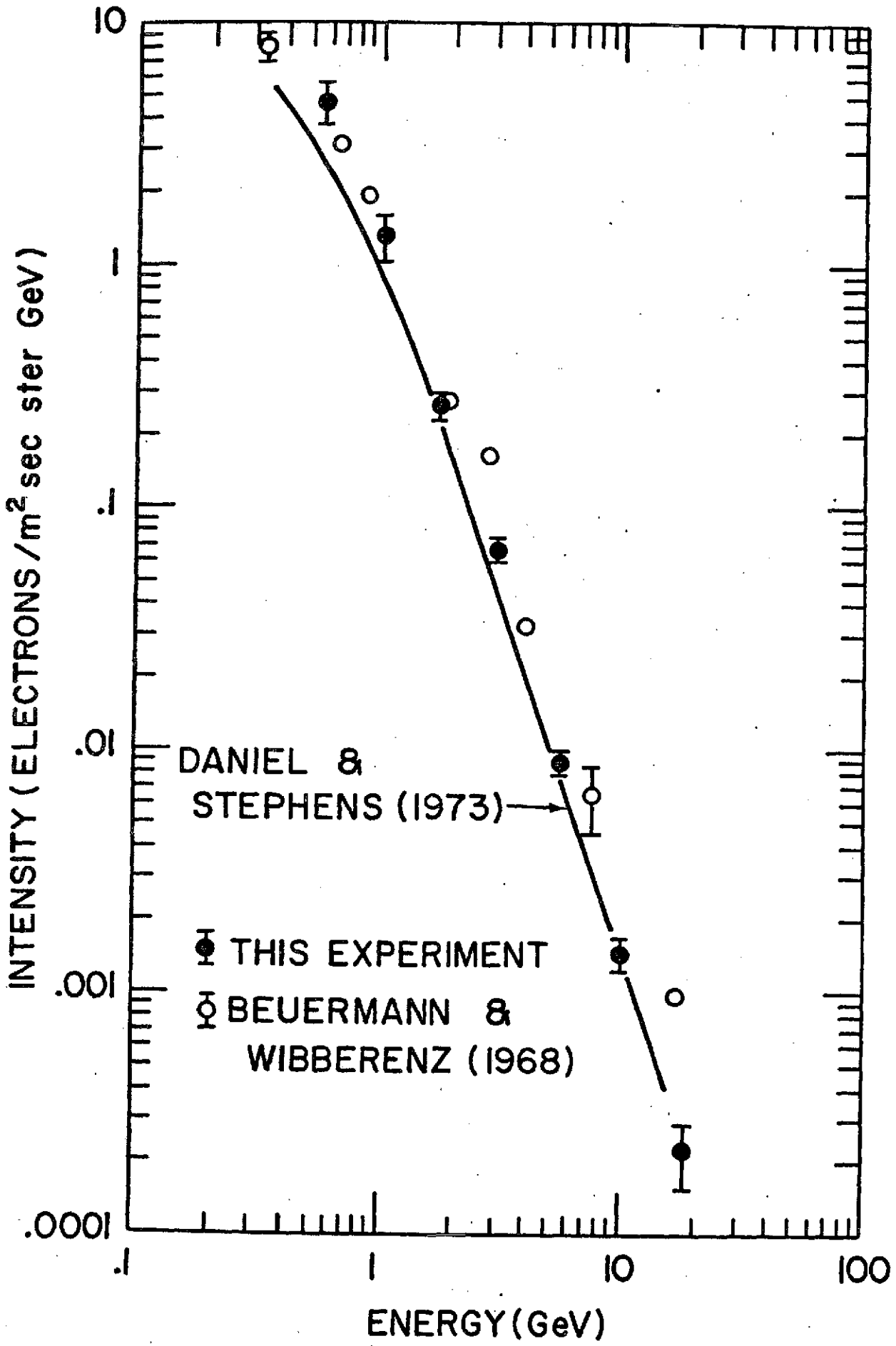
10
1
.1
.01
.001
.0001
INTENSITY (ELECTRONS/m² sec ster GeV)
DANIEL &
STEPHENS (1973)
THIS EXPERIMENT
BEUERMANN &
WIBBERENZ (1968)
.1
1
10
100
ENERGY (GeV)

Figure 16